Distribution Agreement

In presenting this thesis as a partial fulfillment of the requirements for a degree from Emory University, I hereby grant to Emory University and its agents the non-exclusive license to archive, make accessible, and display my thesis in whole or in part in all forms of media, now or hereafter now, including display on the World Wide Web. I understand that I may select some access restrictions as part of the online submission of this thesis. I retain all ownership rights to the copyright of the thesis. I also retain the right to use in future works (such as articles or books) all or part of this thesis.

Olivia Boyd April 28, 2020

Design and Construction of a Tensile and Shear Strength Testing Apparatus to Study the Addition of Fumed Silica to the Acrylic Adhesive B-72 Used in Art Conservation

by

Olivia L. F. Boyd

Connie B. Roth
Advisor

Physics

Connie B. Roth
Advisor

Renee A. Stein
Advisor

Effrosyni Seitaridou
Committee Member

2020

Design and Construction of a Tensile and Shear Strength Testing Apparatus to Study the Addition of Fumed Silica to the Acrylic Adhesive B-72 Used in Art Conservation

By

Olivia L. F. Boyd

Connie B. Roth

Advisor

An abstract of
a thesis submitted to the Faculty of Emory College of Arts and Sciences
of Emory University in partial fulfillment
of the requirements of the degree of
Bachelor of Science with Honors

Department of Physics

Emory University

2020

Abstract

Design and Construction of a Tensile and Shear Strength Testing Apparatus to Study the Addition of Fumed Silica to the Acrylic Adhesive B-72 Used in Art Conservation

By Olivia L. F. Boyd

The field of art conservation adds fumed silica (FS) to acrylic adhesives in order to improve their rheological properties during application. However, little is known about how this added FS may alter the polymer's material properties. Since 1986, when Stephen Koob published an article on how to make the acrylic B-72 easier to work with, which included adding 0.1 wt% FS to the application solvent, B-72 has become very popular in the conservation community. Paraloid B-72 is a copolymer of methyl methacrylate and ethyl methacrylate, with 2.2 wt% butyl methacrylate. In polymer materials engineering, nanoparticles (NPs) are often added in small quantities to increase the modulus and improve strength of the polymer material. These polymer nanocomposites (PNCs) are used today in a wide variety of applications, yet the underlying scientific mechanism by which these nanometer sized particles act to reinforce the material are unclear. While early theoretical work suggested that adding NPs to polymers should increase their glass transition temperature T_g when attractive interactions exist, current experimental work often shows that the average T_g of the polymer matrix is not altered. We confirm this finding for our system via ellipsometry measurements of the glass transition temperature T_g of neat B-72 and B-72 with 0.2 wt% FS (relative to the dried polymer). We then designed and built the Conservation Adhesive Tensile-to-Shear (CATS) tester to determine the fracture stress of adhesives used in art conservation. We determine that the CATS tester produces reproducible data, and obtained preliminary data that suggests that adding fumed silica to B-72 does increase its tensile fracture stress.

Design and Construction of a Tensile and Shear Strength Testing Apparatus to Study the Addition of Fumed Silica to the Acrylic Adhesive B-72 Used in Art Conservation

By

Olivia L. F. Boyd

A thesis submitted to the Faculty of Emory College of Arts and Sciences
of Emory University in partial fulfillment
of the requirements of the degree of
Bachelor of Sciences with Honors

Department of Physics

Emory University

2020

Acknowledgements

I am endlessly grateful to Alan Rohrbach, who was my sounding board throughout this process. I also must thank everyone else in Roth Lab for making my two years with the lab a time of such personal and academic growth. Thank you to Benjamin Kasavan for showing me the ropes, teaching me about polymers in conservation, and starting this work. Thank you to Renee Stein and Jessica Abel for teaching me about conservation and being wonderful sounding boards. Thank you to Effrosyni Seitaridou, who inspired my love of physics and is serving on my committee. Thank you to Horace Dale III and Alan Fannin at the Emory Physics Machine Shop for their superb work in constructing the CATS tester and the drying rack. I want to thank my family and friends for their love and support through my entire college experience. Finally, thank you so much to Connie Roth, who has been an invaluable mentor and teacher in my last two years working for her.

Table of Contents

List of Tables

List of Figures

CHAPTER 1
INTRODUCTION

1.1 Motivation

In the field of art conservation, important historical artifacts are preserved and restored for future study and appreciation. The goal of preserving the original state of the artifact as much as possible while making it more structurally sound leads to four key principles for adhesives: stability, reversibility, imperceptibility, and similarity in strength to the object.[34,36] To be used in art conservation, an adhesive must be chemically stable, not impact the work's visual appearance or the visual experience of the viewer, reversible, and be similar in strength, but not stronger, to the object it is being used on.[34,36] Knowing the strength of the adhesive is vital, as the adhesive cannot be stronger than the object, otherwise if the object is placed under enough stress it will break at a new location in the artifact instead of at the bond. However, too weak an adhesive bond reduces the structural integrity of the entire object.

These four key principles can be connected to measurable physical properties. The index of refraction of the polymer determines how light interacts with a material. By matching the index of the adhesive to that of the artifact, bonds can be made to seamlessly blend in with the object and not impact the visual experience of the object. Next, the reversibility of the bond depends on the glass transition temperature, T_g, of the material. T_g is the temperature on cooling at which the material transitions from a highly viscous, rubbery liquid (a rubber) to an amorphous solid (a glass).[19,38] The temperature dependence of the density (or alternatively the index of refraction) of the polymer has different slopes in the rubbery and glassy regimes, and thus can be used to locate T_g. The last key principle, the strength of the bond, which is affected by the temperature relative to T_g, can be measured as the fracture strength of the bond. Thus by measuring the refractive index, glass transition temperature, and the fracture strength of adhesives, the suitability of polymers for

use in art conservation can be determined.

Adhesives are made from an acrylic polymer resin dissolved in a solvent. As conservators do not heat the bonds to help drive out solvent for fear of damaging the artifact, the T_g of the polymer determines how the polymer material of the bond settles as the solvent evaporates.[19] When a material has a lower T_g then at room temperature the polymer is still able to relax, allowing the bond to densify and strengthen. A higher T_g means that when the solvent evaporates out the polymer cannot relax, creating a porous and brittle material.[19] Thus determining the T_g of an adhesive can indicate how strong a bond it will form. The fracture strength, the amount of stress needed to cause failure in the material, is a fuller measure of the strength of a bond. The fracture strength will be affected by both the plasticizing effects of any remaining solvent, as well as the inherent strength of the polymer itself. Additionally, adhesives with a lower T_g are generally easier to reverse, as less solvent will be necessary to soften the bond.

Paraloid B-72, a thermoplastic acrylic resin, has long been known to be a safe adhesive to use on artifacts, as it is highly reversible and chemically stable.[4,34] However, before 1986 it was considered too difficult to use because of its long drying time and high viscosity, and thought to be too weak to use on its own.[25] Conservator Stephen Koob changed this mindset with his seminal paper on the best way to prepare and apply B-72.[25] He suggested a new procedure for preparing the adhesive, which he claimed would make it easier to work with.[25] Koob recommended making a 1:1 weight ratio of B-72 to acetone solution, with 0.1 weight percent (wt%) of fumed silica (FS) added relative to the total weight of the solution.[25] (In the conventions used in polymer physics, the wt% of added particles is in reference to only the polymer content, and so this would correspond to 0.2 wt% of FS to the total weight of the polymer matrix once all the solvent has evaporated.) To get to a 1:1 weight ratio of B-72 to solvent, a 1:2 weight ratio of B-72 to acetone solution is made, and once the polymer has dissolved, 50 wt% of the acetone is evaporated off. Koob claimed that the 0.1 wt% of FS in the solution helped make the B-72 solution easier to work with by making it thixotropic, which functionally means the adhesive would spread more easily onto the materials to be joined, but not drip after it had been applied.[25] To convince conservators to use B-72 as a

solo adhesive, he then demonstrated the strength of the adhesive by measuring the tensile fracture strength of B-72 applied in this manner.[25] This paper helped popularize B-72, and now it is one of the most common adhesives used in art conservation.[34] However, as 0.1 wt% of FS is such a small amount, many conservators skip adding FS to B-72, not recognizing the role it may play in the physical behavior and strength of the adhesive.[43]

Adding nanoparticles (NPs) such as FS to a polymer such as B-72 creates what is called a polymer nanocomposite (PNC). Due to the extremely small dimensions of the NPs, adding even a small wt% to a polymer matrix can drastically change the macro-scale material properties.[55] NPs reinforce the surrounding polymer matrix, increasing the strain-to-failure of the material.[31] However, typically the T_g of the material is altered by a surprisingly small amount upon the addition of NPs. Previous experimental work has been done on the T_g of PNCs on a system chemically similar to B-72 and FS: PNCs composed of poly(methyl methacrylate) (PMMA) and silica nanospheres.[37] Torkelson et al. investigated how adding different loading levels of silica nanospheres to PMMA changed T_g, and found the nanospheres had a smaller than expected effect on the measured T_g.[37] Theoretical work suggests this is because the methods used to measure T_g measure the majority of the polymer matrix and thus will not show the effect the NPs have on the polymer immediately surrounding it.[42] The measured T_g value occurs when the majority of the polymer matrix transitions.[42] Thus, PNC literature suggests that adding NPs to a polymer could meaningfully alter some material properties that conservators care about, such as the fracture strength, while leaving T_g relatively unaltered.

Until recently, B-72 and other acrylic adhesives had been used more frequently in the conservation of small works, such as ceramics and small sculptures, but not in monumental stone works, as it was not considered strong enough.[34] This paradigm shifted with the work of Riccardelli et al., who tested the interfacial fracture toughness, an alternative measure of strength, of multiple acrylics, including B-72.[36] They showed that these adhesives could actually match the strength of marble, and thus were an excellent adhesive choice for large-scale sculptures.[36] This discovery has lead to a renewed interest in studying the properties of acrylics and has challenged

old assumptions about where they can be safely used.[4]

1.2 Goals of Thesis

Knowing the exact material properties of the adhesives being used in a given project is critical for conservators because any adhesive used in art conservation must fulfill four key properties: chemical stability, reversibility, imperceptibility, and similarity in strength to the object.[34,36] B-72 has been proven to meet these stringent requirements over years of research.[16,25,34,36,4,23,19] Currently, some conservators do not add 0.1 wt% FS to the adhesive solution as suggested by Koob, because his reason for adding the FS was only to make the adhesive solution thixotropic and therefore easier to apply.[25] As such, if a conservator is not having trouble applying the B-72 adhesive, they see no reason to add the FS. Additionally, the amount of FS added is so small, it may seem illogical that it could have any major impact on the performance of B-72. However, insights from the field of polymer nanocomposites suggest that adding nanoparticles such as FS to a polymer such as B-72 could cause large changes in the strain-to-failure and therefore fracture strength of the material, without significantly changing its T_g.[31,42] In this thesis, we seek to determine if adding Koob's 0.2 wt% FS to B-72 (the percentage FS remaining relative to the polymer after the solvent has evaporated) alters any of its properties that would impact its use in art conservation. Furthermore, if the FS does alter any of the properties of B-72, we want to identify what loading level of FS optimizes the material for use in conservation. In this work, we build a device that stresses a bond until it breaks and use it to test B-72 loaded with varying percentages of fumed silica. We also prepare thin-film samples of B-72 with varying percentages of FS and measure its T_g and index of refraction using ellipsometry to determine if there are any changes in those parameters.

CHAPTER 2
MATERIALS AND METHODS

2.1 Materials

2.1.1 Polymer Properties

A polymer is a long chain molecule composed of repeating units called monomers.[38] An important property of polymers relevant to this thesis is their glass transition temperature. Above a polymer's glass transition temperature it is an equilibrium liquid, called a rubber. However, as the polymer is cooled down, it falls out of equilibrium and becomes a transparent, amorphous solid called a glass. The polymer falls out of equilibrium because it does not have enough energy to be able to explore all possible configurations, and becomes energetically trapped. The temperature on cooling at which the polymer becomes a glass is called the glass transition temperature, T_g. Figure 2.1a shows how the volume of a polymer changes on cooling, and defines T_g. Figure 2.1a also illustrates that the value of T_g can change (by a few degrees) depending on how quickly the polymer is cooled.

A polymer dissolved in a solvent can also undergo the glass transition at room temperature, as shown in Figure 2.1b. Commonly used solvents have a very low T_g, and so the mixture of solvent and polymer has a T_g in between that of the solvent and polymer which is typically below room temperature.[19] As the solvent evaporates off, there is less solvent to depress the T_g of the polymer, and so the T_g of the solution rises. Eventually, enough solvent will evaporate off that the solution's T_g will be at room temperature or above, and so the solution will become glassy. This process is called a "solvent quench".

Looking at Figure 2.1, it is evident that many properties of polymers behave differently in the rubbery and glassy regimes. Figure 2.1 a and b concern the temperature or solvent content dependence of the volume, which can be related to the height of the polymer sample. The volume

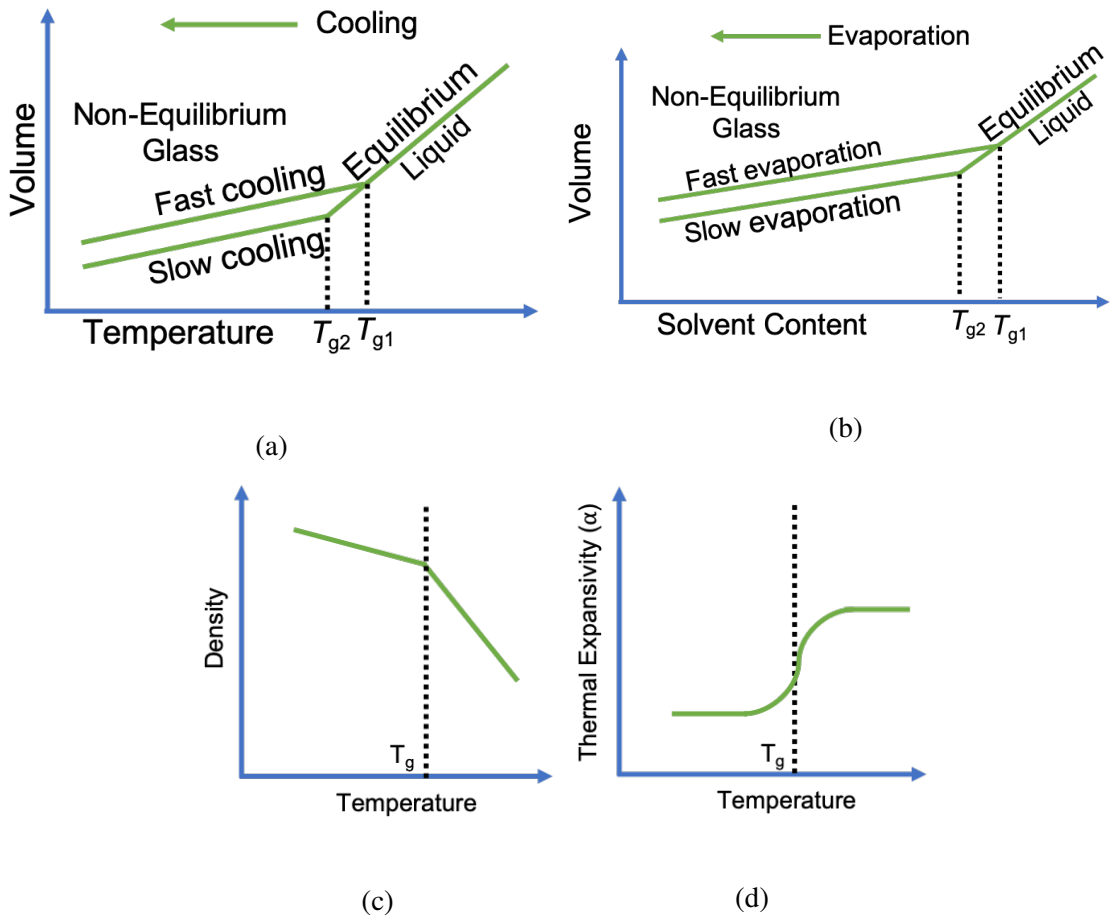

Figure 2.1: Schematic diagrams representing property changes at the glass transition. (a) Volume vs temperature for two different cooling rates of a polymer. (b) Volume vs solvent content for two different evaporation rates of a polymer solution. (c) Density vs temperature for a polymer measured on cooling. (d) Thermal expansivity vs temperature for a polymer measured on cooling.

of the polymer sample is its area times its height, and the area of the polymer will not change as it is adhered to the silicon substrate. Thus, when the thickness of the polymer film is measured, it will behave like the volume of the polymer. By locating the temperature at which the slope of the volume changes with respect to temperature one can determine T_g. Figure 2.1c shows the temperature dependence of density for a polymer measured on cooling. The density as a function of temperature is linear in both the rubbery and glassy regimes, but with different slopes. The density therefore can also be used to determine the T_g of the material. The refractive index is a proxy for the density of the sample. Finally, Figure 2.1d depicts the thermal expansivity vs temperature for a polymer measured on cooling. The thermal expansivity is the derivative of $V(T)$, the volume as a

function of temperature, and so constant in the glassy and rubbery regimes, and the T_g is found in the middle of the transition between the two plateaus. The thermal expansivity can be used to gain further insight into the rapidity and breadth of the glass transition.

2.1.2 Polymers in this Study

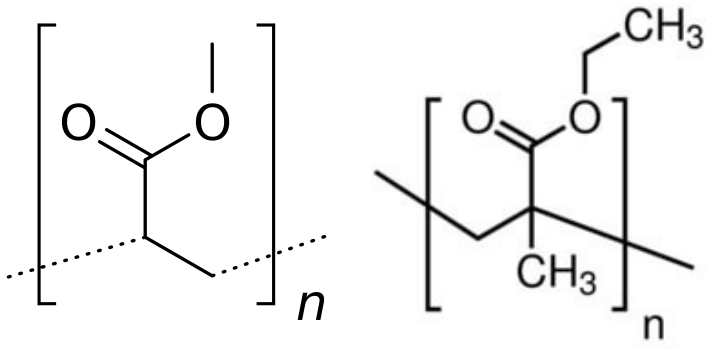

(a) (b)

Figure 2.2: Drawings of the monomers that make up B-72. (a) Methyl acrylate, which would form poly(methyl acrylate) or PMA if it was made into a homopolymer.[13] (b) Ethyl methacrylate, which would form poly(ethyl methacrylate) or PEMA if it was made into a homopolymer.[35]

The acrylic polymer we are examining is Paraloid B-72, a polymer produced by Rohm and Haas. B-72 is composed of 32% methyl acrylate (MA), 65.8% ethyl methacrylate (EMA), and 2.2% butyl methacrylate (BMA).[4] The monomers of PMA and PEMA are shown in Figure 2.2. If a homopolymer of EMA was made, it would have a T_g of 65 °C, and a homopolymer of MA would have a T_g of 10 °C.[10] B-72 has a T_g of 40 °C, which is between the T_g of homopolymers made of the monomers EMA and MA. The large difference in the T_gs of the constituent monomers likely contribute to the broad glass transition seen in B-72.[23] The solvents acetone, toluene, xylene, and p-xylene are often used to make solutions with B-72.[4,19,12] When used with fumed silica (FS), acetone is the most commonly used solvent, as it evaporates very quickly.[25,34,40,4] B-72 has a refractive index of 1.48 when measured at the literature standard of $\lambda = 598$ nm, the sodium D line.[19]

B-72 is used so frequently in art conservation because it is extremely stable and reversible, and it has been tested and found acceptable for use in conservation.[4] Art conservators use the Feller system, which rates materials in terms of how long they will be photochemically stable.[4]

B-72 is a Class A material, meaning it is excellent for use in conservation, and the intended useful lifetime of the material is greater than 100 years.[16] Because of its Feller rating and large presence in the literature, B-72 is used in most conservation applications. However, in this work we are only examining the functionality of B-72 as an adhesive.

In contrast, Paraloid B-44 is a much more specialized polymer, as it remains stable, soluble, and reversible for much less time but is tougher than B-72.[4] It is composed of 28 wt% ethyl acrylate and 70.3 wt% methyl methacrylate,[4] with a T_g of 60 °C.[4] While B-72 has a Knoop hardness of 10-11, B-44 has a Knoop hardness of 15-16.[4] This higher T_g and hardness directly contribute to its niche purpose. B-44 is a key ingredient in Incralac, which is used as a protective, transparent coating for objects made of copper and silver alloys, and resists weathering and corrosion on objects displayed outdoors.[32] However, after around ten years, Incralac becomes cross-linked (bonds form between separate polymer chains), and thus becomes insoluble and therefore irreversible in a conservation context.[15] In this work we research the physical properties of B-44 and connect them to the properties such as hardness and T_g that conservators care about.

2.1.3 Fumed Silica

Fumed silica (FS) is a mixture of small, spherical particles and fractal structures. These geometries are key to understanding its ability to provide structural reinforcement to polymers and make the solutions to which it is added thixotropic. Both the spheres and fractals are formed in the same manufacturing process, where silicon tetrachloride is oxidized in a high temperature flame, creating a silicon dioxide vapor.[6] This vapor coalesces into molten droplets.[6] There is then a delicate balance between the forces of surface tension and viscous resistance as the molten particles move through the flame, carried by an inert gas such as nitrogen.[6,5] As the viscosity of silica is highly dependent on temperature, the size of these initial molten droplets can be controlled through altering the flame's temperature.[6] The flame is chaotic, causing temperature fluctuations in the manufacturing process, resulting in a wide distribution of droplet sizes.[6] These droplets, once solidified, are termed primary particles. Once the droplets cannot get any larger,

collisions between particles result in adhesion between droplets, creating fractal structures of connected droplets called aggregates. Not all droplets end up fusing, so 40-60% of any given FS sample will be composed of isolated, nano-size, spherical primary particles.[41] All particles then exit the hot part of the flame and cool below the fusion temperature of silica.[41] Both the fractal and spherical particles will continue to collide, becoming mechanically and reversibly stuck together in groups called agglomerates.

The primary particles of the FS we use in this study are between 7-14 nm in diameter,[41,8] and form aggregates around 100-200 nm long, composed of 10-30 fused primary particles.[41] FS is naturally hydrophilic due to the presence of hydroxyl groups on the FS surface.[41] While FS can be further processed by reacting the hydrophilic silanol groups with organic groups, making the overall particles hydrophobic, in this study we will be using hydrophilic fumed silica, as that is what the Carlos Museum uses.

2.2 Weight Percent Conventions

The fields of polymer physics and art conservation have different conventions in how the concentration of filler particles are reported. In the polymer nanocomposites field, the concentration relative to the final, dried material is reported. For example, if the FS was 1% by weight, that would mean that the polymer matrix was composed of 99% polymer and 1% fumed silica by weight. These wt% can be converted into volume % using the density of the materials. The density of amorphous silica is approximately 2.2 g/cm^3. We will estimate B-72's density as around 1 g/cm^3, as it is made of mostly MA and EMA, which both have a density of approximately 1 g/cm^3. 1 wt% FS in 99 wt% of B-72 is thus equivalent to 0.46 vol% of FS in 99.34 vol% polymer. In conservation, there are multiple different ways of reporting the nanoparticle percentage, including weight % and volume %. Byrne and Koob report their weight percentages as the percent of the total solution.[25,7] In Koob's adhesive preparation method, he suggests making a 50% acetone, 50% B-72 solution, and then adding 0.1 wt% FS to the solution.[25] In the convention used by the polymer nanocomposite field, this would be 0.2 wt% of FS in B-72. A few papers do not

specify the percentages used,[26,27,18] while others use a (weight of polymer)/(volume of FS) as a percentage.[33] Still other papers use the polymer nanocomposite's convention.[56,19,54] In this thesis, we will be using the polymer nanocomposite's conventions, reporting the quantity of nanoparticles as a weight percentage of the final product, since in the adhesive bonds the solvent evaporates off, leaving behind only the polymer and nanoparticles, a polymer nanocomposite.

CHAPTER 3

RELEVANT LITERATURE

3.1 Polymer Nanocomposites

Polymer nanocomposites (PNCs) are created by adding nano-sized, typically inorganic, particles to a polymer. Usually only a couple weight percent (wt%) or less of the nanoparticles (NPs) are added, however even this small amount of material provokes large changes in some of the material properties of the polymer matrix.[31] Typically, PNCs show increases in measurements of strength, such as the fracture strength, the yield stress, and the elastic modulus (e.g. Young's modulus for tensile deformations).[31] Such small amounts of an additive are able to have such a large impact on these properties if the particles are very small and well dispersed.[31]

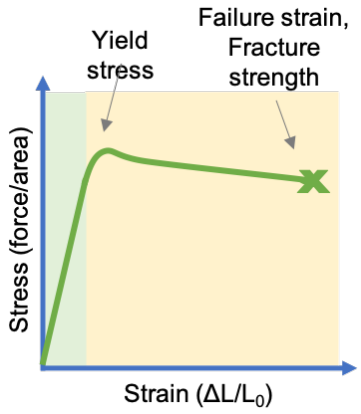

Figure 3.1: A generic stress-strain curve for thermoplastic polymers. The green section of the graph is where the polymer deforms elastically, and the yellow section is where the polymer deforms plastically. The yield stress is the stress at which the material stops deforming elastically and begins plastic deformation. The elastic modulus is the slope of the stress-strain curve in the elastic regime. The X indicates at which stress and strain the material fails. The x coordinate of this point is the failure strain, and the y coordinate is the fracture strength.

There are many different ways to define and measure the "strength" of a material. Figure 3.1 shows a schematic plot of stress vs strain that depicts the typical relationship between the two for a thermoplastic polymer. The figure also defines the fracture strength, the failure strain,

and the yield stress. The fracture strength is the minimum force per area required to break the material.[19] The failure strain is a measure of how much a material is able to stretch or deform before breaking.[19] The yield stress is the force per area at which the material stops deforming elastically, meaning reversibly, and begins to deform plastically, meaning irreversibly.[19] The elastic region of the stress-strain curve is in green in Figure 3.1, and the plastic region is in yellow. Young's modulus is the slope of the elastic portion of the tensile stress-strain curve.[19] Young's modulus is a property of the material which describes its elastic deformation properties. Given a stress applied in a uniaxial deformation, Young's modulus gives the resulting strain. In this thesis we will be using the fracture strength as our measure of strength, because that is a common metric for studying strength in art conservation.[25,34,40,33]

Figure 3.2: This kg of 1 mm^3 particles has the same surface area as this mg of 1 nm^3 particles.[57]

Although the exact mechanism for how the NPs reinforce the surrounding polymer matrix is not entirely known, current theories suggest that some of the polymer matrix strongly interacts or adheres to the nanoparticle. This affected region or thickness of the polymer matrix around the nanoparticle, called the "interfacial volume" or "bound layer" has different properties than the bulk polymer.[21] Therefore, to maximize mechanical reinforcement, one must maximize the surface area of the NPs that will interact with the polymer matrix. In general, the bound layer is independent of particle size.[55] The nano size of the particles added to the polymer matrix is essential because for the same volume or weight added, nano particles are far more numerous, and thus are closer to each other and have a larger total surface area compared to micro-sized particles.[55] The relationship between the size of particles and their surface area are illustrated in Figure 3.2, which shows two

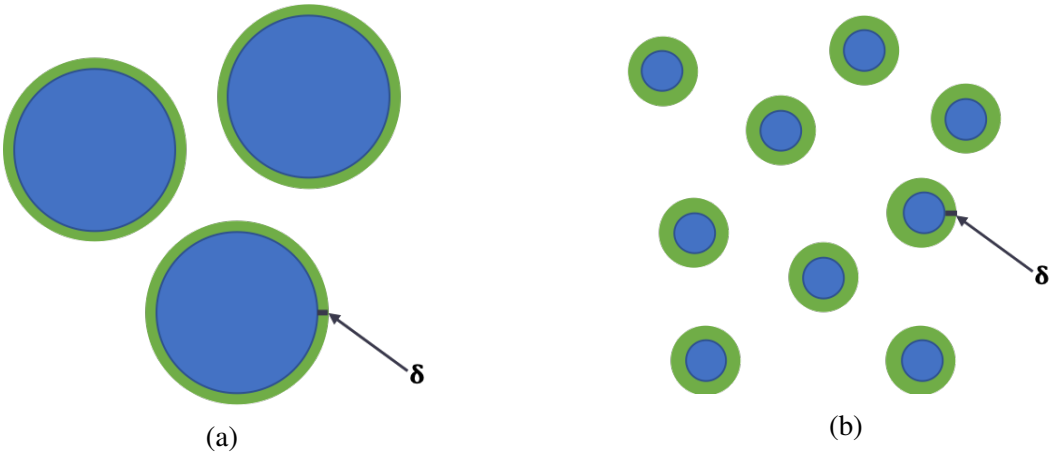

Figure 3.3: The relation between particle size and interfacial volume. As the width of the interfacial thickness δ around the nanoparticles is independent of particle size to the first order,[55] the amount of polymer affected by a given mass of particles depends on their surface area. The particles are pictured in blue and the interfacial volume is depicted in green. These two figures are not to scale with each other.

sets of particles that have the same total surface area. It takes 10^6 times more mass of mm^3 particles to match the surface area of nm^3 particles. Figure 3.3 further illustrates this point. The figure shows that when the particles become nanoscale, a much larger volume of polymer will be affected by the nanoparticles than by an equivalent mass of microparticles, since the size of the particle does not change the thickness of the bound layer, but the greater number of particles increases the surface area.

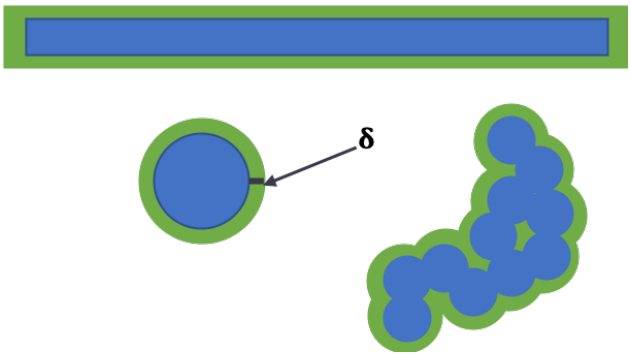

Figure 3.4: The relations between particle shape and interfacial volume. For a given interfacial thickness δ around the nanoparticles, the amount of polymer affected by the particle depends on the geometry of the particle. Pictured here are cross sections of three different particles in blue: a rod, sphere, and an aggregate of spheres with a fractal shape. The interfacial volume is depicted in green. The sphere has the smallest ratio of particle volume to interfacial volume compared to the aggregate of spheres and the cylinder.

Several different possible nanoparticle geometries are depicted in Figure 3.4. The geometry of the nanoparticles in blue alter the size of the interfacial volume in green. Spheres have the smallest interfacial volume (surface area) per unit volume. Cylinders and plates have a much larger surface-to-volume ratio. In this study, fumed silica (FS) is being used, which is 40-60% fractal shaped aggregates, and 40-60% spherical primary particles.[41] The fractal shaped aggregates are made of bonded spherical particles, and thus can be thought of as existing between the surface-to-volume ratio of spheres and cylinders. The spherical primary particles have smaller surface area to volume ratio, but because these primary particles are around 10 times smaller than the aggregates, they will still affect a significant portion of the polymer. FS also has an increased surface area to volume ratio due to its porosity, and will therefore have a large surface area compared to the particle volume.

As there is still so much unknown about how PNCs work, this study will inevitably run into some of the open questions in the field. For example, while the solvents used in this study will be determined by art conservation's best practices, we will be unable to fully explain how the casting solvent affects the dispersion of the nanoparticles in the solvent-quenched polymer matrix.[28] Additionally, while some experimental studies can help set our expectations as to how the fractal and spherical FS particles will affect the surrounding polymer matrix,[22,21,31,37] there is limited theoretical work that explains how the bound layer affects the bulk properties of the polymer.[28] Finally, only a small fraction of the experimental work on PNCs has focused on how NPs alter material properties while in the glassy state, which is what we are focused on in this work.[28] Thus, while we will be able to inform the field on how adding FS to B-72 affects the material properties of the acrylic, further advancements in the PNC field will be valuable in continuing to understand these effects.

3.1.1 Property Changes in Materials with the Addition of Nanoparticles

Adding nanoparticles to a polymer matrix affects the elastic modulus, the yield stress, and the fracture strength, but changes the glass transition temperature T_g much less than expected.[31]

The elastic modulus describes the resistance of the material to being reversibly deformed, and is generally increased by the addition of NPs.[31] Yield stress measures how much stress is required to permanently deform a material, and is usually reduced by NPs.[31] The strain at fracture or ultimate strain is the maximum amount the matrix can deform before it fails.[19] Adding nanoparticles drastically increases this property.[31] The ultimate strain is a commonly measured property in the PNC literature, but for conservation the fracture stress matters more, as that describes the amount of stress needed to break the bond. The ultimate strain is closely related (but not necessarily correlated with) the fracture stress, and so it is not unreasonable that the addition of NPs could have a large impact on the fracture stress of a material. Given the huge impact that adding NPs has on many of the macro-scale properties of the PNC, it is surprising that the glass transition temperature, T_g, has been found to be largely unaffected by the addition of NPs.[37,30,1]

In their 2013 paper, Maillard et al. investigated the impact on measures of material strength due to adding silica NPs grafted with polystyrene (PS) chains to a PS matrix. Young's modulus, yield stress, and failure strain were measured at different loading levels of NPs.[31] Maillard et al. found that in a glassy system, adding more NPs did not monotonically increase the strain at failure.[31] Instead, the failure strain peaked at around 5 wt%, with a sharp decrease for larger loading levels.[31] Investigating why there was a marked decrease in failure strain after 5 wt%, Maillard et al. imaged samples with different loadings of 14 nm diameter colloidal silica (simple spherical particles) using transmission electron microscopy (TEM) and found that past a critical point of NP loading, the NPs start to form connected superstructures in the matrix.[31] Maillard et al. found from TEM images taken at the failure point that when the nanoparticles had not formed superstructures, they were able to move in response to the stress, thus releasing energy.[31] However, once superstructures had formed, the NPs could not reorganize themselves, which stopped the material from being able to form shear bands as a response to the strain, and so the material had a brittle failure originating with the NPs.[31] Cracks in the material began near polymer-NP interfaces, thus suggesting that the NPs were actually causing the decrease in strain-to-failure measured.[31] The loading percentage and dispersion of the NPs control superstructure formation, and therefore

can be varied to maximize the increase in strain-to-failure imparted by the NPs. Maillard et al.'s finding suggests that it is important to ensure that the NPs are dispersed throughout our system in order to get the largest increase in strain-to-failure for a given wt% of NPs. Although Maillard et al. were looking at nanoparticles of silica spheres with chains grafted on them and our system does not have grafted chains, our systems are similar enough that we expect their findings of superstructure formation and crack creation to apply, and thus we predict a similar non-monotonic pattern in the strain-to-failure vs loading level in our system.

The loading percentage at which NPs will form a superstructure that spans the material, also known as percolation, is highly dependent on particle shape. In experimental work by Zhao et al., it was extrapolated from experimental data using rubber elasticity theory that the percolation threshold of their FS was 3.7 vol%.[58] Zhao et al.'s FS had aggregate lengths around 0.1 microns longer than the FS we use, and had its surface treated with dimethyldichlorosilane.[58] Knowing that the density of amorphous silica is 2.2 g/cm^3 and the density of the poly-(2-vinyl-pyradine) (P2VP) used is approximately 1 g/cm^3,[52] 3.7 vol% is determined to be equivalent to about 7.8 wt%. This extrapolation is backed up by a theoretical estimate of maximum packing volume fraction from Cassagnau et al.[58,9] Comparatively, the percolation threshold for colloidal silica was estimated to be 16 vol%,[58] or around 30 wt%. Zhao et al. attributed this disparity in loading levels to reach percolation to the large differences in shape between the FS and colloidal silica.[58] As determined by Maillard et al., reaching percolation reduces the mechanical reinforcement of the material in the glassy state,[31] so it is likely the largest increase in fracture strength will occur when less than 7.8 wt%. of FS is added to a polymer.

3.1.2 Bound Polymer Layer

One of the biggest open questions in the polymer nanocomposite literature is the mechanism through which adding small quantities of nano-sized particles to polymer matrices produces such large macroscopic changes in measures such as failure strength.[28] It is theorized that these changes come from the NPs perturbing the nearby polymer matrix as mentioned earlier (see the

beginning of Section 3.1).[17] The terms "interfacial thickness" and "bound layer" are used to describe the layer of perturbed polymer around the nanoparticle.[55,28] However, the exact width of that layer is an area of current research.[21] In a paper by Jouault et al., in which various methods of measuring the bound polymer layer are used, a wide range of possible widths were found, ranging from 3-20 nm.[21] This spread of values is not surprising given that different measurement techniques measure the polymer layer of interest in different conformations.

Currently, the NPs are thought to perturb the polymer surrounding the NPs by providing an obstacle to polymer movement.[17] Polymers near a NP are unable to move in all directions, which slows down their dynamics,[11] and could result in a higher fracture strength measure due to an increased rigidity in the material. Further support for this interpretation comes from glycerol, which is not a polymer but still has altered properties and a measurable bound layer upon the addition of NPs.[11] Thus, the mechanism through which a bound layer is formed cannot rely on polymer-specific properties. This argument is able to explain both the perturbations in the polymer matrix and the glycerol solution.

Understanding the bound layer is key to determining why adding NPs to a polymer does not alter the T_g of the material as drastically as would be expected given findings in thin film systems. Studies of T_g as a function of distance from a substrate have shown that T_g can be altered by a nearby interface.[38,2,14] It was thus suggested that the T_g of PNCs could be different from the neat (no additives) polymer's bulk T_g.[42] This prediction was made because each NP creates an interface with the polymer, and a critical aspect of PNCs is the large surface area of NPs relative to their volume. However, it was found experimentally that the T_g of PNCs was only minorly altered compared to the neat polymer.[37,1,30] In 2016, Starr et al. conducted simulations of PNCs with different NP-polymer interaction strengths to elucidate the mechanisms behind the unaltered T_g values.[42] They found in their models that when the polymer-NP interaction strength is larger than the polymer-polymer interaction strength, the NPs develop a bound polymer layer that "decouples" from the polymer matrix, effectively "cloaking" the broader polymer matrix from the perturbation caused by the interface.[42] Starr et al. suggested that as most current experimental techniques measure the

T_g of the majority of the polymer matrix, these bound layers that do experience a different T_g are insufficient to change the measure of the average T_g of the sample.[42] Thus in our B-72 and FS system, we do not expect to see a change of B-72's bulk T_g of more than a few degrees Celsius upon the addition of FS.

A separate phenomenon called adsorption may also play a role in the dynamics seen in this thesis. Adsorption of polymer chains to surfaces is well-characterized in solution, where polymers attach to a substrate placed in the solution.[17] Polymer chains attach to the substrate in various conformations.[17] Once a polymer is attached to a section of the substrate, that polymer section can be exchanged, but there is no way to completely remove the adsorbed layer in solution.[48] These conclusions are drawn from the behavior of the extensively studied case of a two-dimensional substrate immersed in solution, which we believe to be analogous to our system of NPs (functionally 3D substrates) suspended in a polymer solution. When we solvent-cast our solution to form an adhesive joint, polymers will adsorb to the NP surfaces, so we expect to find adsorbed layers (i.e. bound layers) in our final PNC. The extent to which polymer chains will adhere to the NP surface in solution will depend on the casting solvent used, and can affect the final properties of the PNC formed even after all the solvent has been removed, as described in the next section.[37]

3.1.3 The Importance of Solvents

While there are only two components to the final PNC, the polymer and the NPs, solvent is used to form the composite. The type of solvent and how it is evaporated off is critical to shaping the final structure of the PNC. A polymer-NP attraction that is stronger than the solvent-NP interaction leads to excellent dispersion of NPs in the PNC as the polymers cluster around the NPs, preventing the NPs from aggregating.[22] However, if the solvent-NP interaction is stronger, then the polymers may be prevented from adhering to the NP surface.[37] If the solvent prevents the polymer from adhering to the NP, this missing interaction between the polymer and the nanoparticle could end up being similar to a free surface (where there is free space at the interface).[37] Free surfaces can have a huge impact on the local T_g of the polymer.[39] Thus if the solvent-NP interaction is

more energetically favorable than the polymer-NP interaction, and if free surfaces actually form at the polymer-NP interfaces, we would expect to see a decrease in the T_g as seen in the study by Rittigstein and Torkelson.[37]

Additionally, as we have already discussed, the bound layer formed from the attraction between the polymers and the NPs is essential to the mechanical improvements seen in PNCs. A solvent that prevents that bound layer from forming due to the solvent-NP interaction being more energetically favorable than the polymer-NP interaction must then also have a serious impact on the strain-to-failure and other strength parameters. Jouault et al. found that choosing solvents that allow the polymer and NP to interact strongly forces the NPs to disperse in the polymer matrix.[22] As acetone can hydrogen bond with the silica surface while toluene cannot, the FS in the B-72 and acetone solution may not be as well dispersed as FS in a B-72 and toluene solution. If the solvent-NP interaction is stronger than the B-72-FS interaction, then we could expect to see the NPs clumping together, impacting the mechanical strength of the PNC bond.

3.2 Art Conservation Literature

Art conservators have the difficult job of working with unique, irreplaceable objects, so much care is put into tailoring the materials and methods commonly used in conservation to the object at hand.[19] Conservators are often not given the time or resources necessary to do the basic research on fundamental properties of the materials they use. There is existing literature on strength testing, solvents, and drying time that will be highly applicable to our research, but not many articles exist that describe research on the properties of the materials they use. Also, while there have been studies that noticed changes in the strength of adhesives upon the addition of FS, these discoveries were mentioned only in passing. No one has specifically studied how FS changes the bond properties of B-72 or other adhesives. However, the following literature can inform us on how different experimental factors should affect our research results.

3.2.1 Effect of Fumed Silica on Material Properties of Polymers Used in Art Conservation

The small portion of the conservation literature that does address the addition of FS to an adhesive primarily considers it as a way to change the viscosity of the solution for the application process of the polymer to the object. In 1984, before the effect of nanoparticles on polymer matrices was discovered by polymer scientists, Byrne wrote a literature review and summary of his own experiences with FS, mainly focusing on how the addition of FS to an adhesive allows the conservator to control the viscosity of the solution, as well as to make the solution thixotropic.[7] The viscosity of thixotropic liquids depends on the shear force felt by the material, where increased force will reduce viscosity and vice versa.[25] This property makes the adhesive much easier to use by conservators, as they can easily mix the solution and wet the application tool, but when the adhesive is applied to the object it will not drip off the break and onto the surface of the artwork.[25] In his paper arguing for the wider use of B-72, Koob champions adding 0.1 wt% FS to a 1:1 B-72 and acetone solution in order to induce thixotropic properties and improve general workability.[25] He stated that larger loading levels did not improve the workability, and when he added 1-5 wt% FS as Byrne cited,[7] he found his bonds were qualitatively "very poor and brittle".[25] In 2001, Podany et al. were also adding around 18 wt% FS to epoxies in order to increase the viscosity of the resin to the desired levels.[34] While using FS to change the viscosity of the solution is common in modern art conservation, some conservators do not add Koob's suggested 0.1 wt% because they consider that amount to be too small to substantially change the properties of the adhesive.[43]

Some papers in the conservation literature have noticed a change in fracture strength when they added fumed silica to various adhesives. Byrne cited data from Cabot Corporation which showed an increase in failure strain when FS was added to an adhesive.[7] However, these tests were done on cotton duck, and none of the data were from thermoplastic adhesives.[7] Therefore these data are not very applicable to the stone, ceramic, and glass conservators that normally use adhesives. In the course of testing adhesive formulations for use in monumental marble sculptures, Podany et al. found that epoxy with FS showed higher fracture tensile strength compared to neat epoxy.[34] To test different adhesives to determine their suitability for use as fills in white marble,

Nagy examined the compressive fracture strength, and found an increase for epoxies with added FS compared to neat formulations.[33] While the increased strength of adhesives with added FS has been noticed in the literature, so far no one has studied if there are any property changes when adding Koob's suggested amount of FS to B-72,[25] corresponding to 0.2 wt% of the dried polymer matrix.

3.2.2 Effect of Drying Time on Fracture Strength

One of the reasons that conservators care so much about how rapidly a solvent evaporates out of the bond is that solvent still in the bond acts as a plasticizer, weakening the bond. Thus if some fracture strength tests are performed on a bond before the solvent has evaporated out, one would get a lower measurement than the actual fracture strength of the bond over the next couple of months. Current studies in this area all test different bond sizes and geometries, which impact solvent evaporation, making it very difficult to compare them.

Before we discuss the conservation literature, the four different types of adhesive failure must be defined. Figure 3.5 shows and names these four types of failure. The blue shapes in Figure 3.5 are the pieces being adhered, and the yellow shapes are the adhesive. In the first case, cohesive failure, the fracture occurs in the adhesive. This mode of failure should only occur at room temperature when there is still solvent in the bond.[40] The second type of failure, adhesive failure, occurs when the adhesion between the adhesive and the object is the weakest part of the system, and thus the adhesive peels off the object without damaging it. The third and forth type of failure are minor and major substrate failure. These failure modes occur when the object itself is the weakest part of the system, and so fracture occurs within it. In minor substrate failure, a crack often forms close and parallel to the adhesive bond. Major substrate failure means the object will be severely damaged if too much force is applied to the system. In conservation, where preserving artwork for future generations is the goal, adhesives that fail cohesively or adhesively to prevent damaging the artwork are desireable.[40]

Koob investigated how drying time changed the fracture strength of the B-72 with FS by

testing the bond after 1 and 3 days of drying.[25] Koob used two glass slides adhered end-to-end. The ends of glass slides are 1 mm by 25 mm. Koob saw huge improvements with the additional two days of drying, as the fracture strength of the bond increased from an average of about 150 kPa to about 600 kPa.[25]

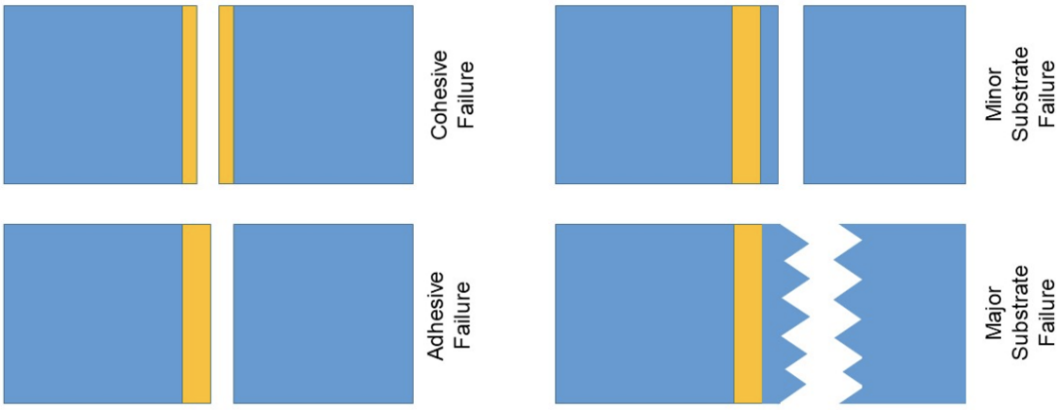

Figure 3.5: Four different modes of failure in adhesive bonds. The blue shapes are the objects being adhered together, and the yellow shapes are the adhesive bond.

Russell and Strilisky measured the fracture tensile strength of several different adhesives at 3 days, 3 weeks, 3 months, 7 months, and 9 months to determine how their strength changed as they dried.[40,25] They actually studied 1:1 B-72 and acetone, which is an excellent match to our system. They tested limestone substrates adhered end-to-end.[40] The ends were 0.75 inches by 2 inches, much larger than Koob's samples.[40] Their samples failed cohesively up to 3 weeks (see Figure 3.5), indicating insufficient solvent evaporation.[40] From 3 months on, the failure was either adhesive or occurred in the limestone right next to the bond. The largest improvements in fracture strength of B-72 occurred in the first three weeks, with diminishing returns for longer drying times. This pattern of drying (quick improvements in the first three weeks, then slower improvements to 3 months) matches the way acetone was observed to evaporate in B-72 by Vincotte et al.[53] Additionally, the improvements in fracture strength as the bond dried follows the increase in observed T_g of B-72 with acetone to above room temperature after around 75 days of drying at room temperature.

Clearly the amount of time the bond has to dry is crucial to evaluating the fracture strength of the bond. However, different articles in the literature use very different rectangular bond geome-

tries. In an attempt to compare these different studies to inform our own experimental design, we propose calculating the exit area for the evaporating solvent, i.e., perimeter of the bond geometry, per mm^2 of the bond area, and using that to standardize how much the samples have been able to dry when they are tested. This idea will be considered further in Chapter 6, when we discuss initial tests conducted to determine design parameters for the device.

3.2.3 The Importance of Solvents

When choosing solvents for use in their adhesives, conservators are concerned about the toxicity of the solvent and how long it takes to evaporate.[19] The toxicity is important because the solvent should not damage the artwork as the adhesive is applied and as it dries out.[19] Bonds are also sometimes applied in locations with less than adequate ventilation, and the health of conservators to repetitive exposure to solvents is a concern.[19] The retention time of the solvent in the polymer is also important, as conservators need their bonds to dry as quickly as possible.[44] There must be a quick drying period, as the object fragments often cannot be clamped and frequently the adhered fragments must be load-bearing soon after the adhesive application.[44] Acetone (nail polish remover) evaporates much quicker than toluene (paint thinner) because of its much lower boiling point and high volatility,[19,47] and it is also less toxic than toluene.[25] Acetone is by far the most commonly used solvent because of these favorable properties, and because Koob strongly advocated for its use in his 1986 paper.[25]

The effects of residual solvent on B-72 can be seen clearly in work by Vincotte et al.[53] In a recent study, they compared the drying times of B-72 in acetone and toluene. They found that after 100 days of drying at room temperature, there was a stable 1 ± 0.5 wt% acetone left in the acetone-B-72 solution. After 150 days of drying at room temperature, there was still 5 wt% of toluene left in the toluene-B-72 sample. This study underscores how long both solvents take to evaporate out of a solution with B-72, and thus indicates that the effects of solvent on the bond will be deeply relevant for up to half a year after application. Vincotte et al. go on to investigate how residual solvent effects the T_g of B-72, finding that with 5 residual wt% of either solvent, the

T_g of B-72 is suppressed to 15 °C. With 1 wt% of residual solvent, the T_g was found to be 34 °C, still lower than the reported value from the manufacturer of 40 °C. This lower T_g indicates a weaker bond that will move and slump much faster. The difference in the drying rate of toluene and acetone additionally emphasizes how much better acetone is as a solvent for conservation, as its faster evaporation means the T_g of B-72 will rise above room temperature much more quickly, allowing it to become a glass that securely bonds artifacts.

Almost no research has been done on the effect of using different solvents on the fracture strength of a bond. However, Podany et al. did test a B-72 adhesive made with acetone or toluene bonding marble under tensile stress and found virtually no difference in the failure strain of the bond.[34] Confirming this finding could be an interesting question to pursue, but it will not be considered in this study. Thus we will use acetone with B-72 for the strength tests due to its lower toxicity and faster drying rate. However, we will use toluene with B-72 for the ellipsometry measurements, as acetone evaporates too quickly and so the film surface is too rough to measure.[23]

3.2.4 Shear vs Tensile Stress

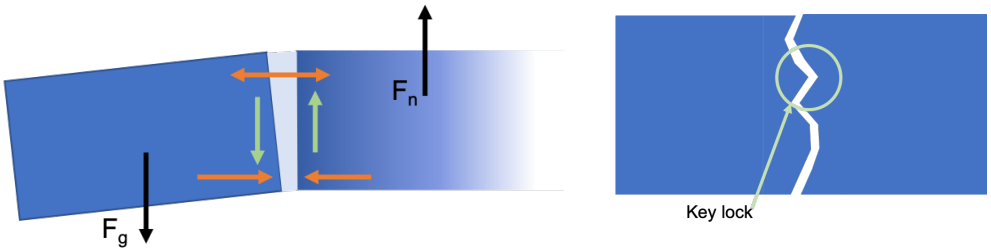

Figure 3.6: (a) Forces on a glued segment of a rod. The gravitational force, F_g, and the normal force, F_n exert torques on the bond, causing tension in the top portion of the bond and compression in the lower half of the bond.[34] These stresses are depicted in orange. The gravitational force also causes shear stress, pictured in green. (b) Key locks. Even when the stress is primarily shear, the rough breaks that are ubiquitous in conservation mean that the joint must pull apart to some extent in order to reduce friction in the joint such that the sides can slide past each other.[34] Thus again the tensile strength of the adhesive determines in part the adhesive's response to shear stress.

Art conservators must mend breaks that occur at any angle, and so the relative shear and tensile strength of their materials need to be understood. Shear stress is when the force exerted

on the material is coplanar with a cross section of the material. Tensile stress occurs when the force exerted on the material is perpendicular to the cross section of the material. Tensile strength ends up being the more important measure due to the roughness of the break. As seen in Figure 3.6, if a break occurs parallel to the ground, tensile forces act on the upper half of the break, and compressive forces act on the lower half.[34] Additionally, the jagged edges that result from a break can create "key locks", which create large frictional forces which oppose the shear force.[34] Thus for the primary stress on the adhesive to be shear, the bond must be pulled apart, so the tensile strength of the material matters even in cases that appear to depend primarily on shear strength.[34] Podany et al. investigated the shear and tensile strengths of neat B-72 ny adhering smooth slabs of marble as part of their 2001 study on the use of B-72 in monumental sculpture conservation.[34] They found that B-72 was much weaker under shear stress than it was under tensile stress, although that may have been because the shear samples had not dried enough.[34] The shear and tensile samples had different bond geometries, so comparing them in terms of drying is not easy. However, comparing the drying time to the exit area per mm^2 of the bond area tells us that both tests were comparable, suggesting that there may be a difference in B-72's fracture strength in shear and tensile. All of the other literature testing the failure strength of adhesives focus solely on tensile stress.

CHAPTER 4
EXPERIMENTAL METHODS: ELLIPSOMETRY

4.1 Ellipsometry Theory

The goal of ellipsometry is to determine the refractive index and the thickness of thin films. The refractive index is a proxy for density, and the film thickness corresponds to the volume of the polymer, as previously discussed in Section 2.1.1. These properties have different rates of change relative to the temperature of the material for a polymer in the glassy or rubbery state, and so both can be used to locate the glass transition temperature T_g, as well as being important in and of themselves. The experimental technique of ellipsometry allows us to gather data that is directly related to the properties we are interested in. We then fit the data collected to a model to get the actual refractive index and film thickness data to analyze.

First let us discuss the design of the ellipsometer. A cartoon depiction of the ellipsometer is shown in Figure 4.1. Unpolarized light is produced from a bulb, and shines through a linear polarizer. The polarized light then passes through the compensator, which is a rotating quarter-wave plate that introduces a phase shift δ between the two components of the light, elliptically polarizing it. The light then interacts with the sample, and then the altered light is received by the analyzer, which takes the elliptically polarized light and reverts it to linearly polarized light. The light finally hits the charge coupled device (CCD) in the detector, which measures the intensity of the light as a function of λ, and then the ellipsometer's software derives two parameters known as Ψ and Δ from the light intensity at the detector. A discussion of how the ellipsometer calculates Ψ and Δ from the information imparted by the incoming light is discussed next.

The ellipsometer uses elliptically polarized light to collect data on the sample. The vector of the total electric field can be decomposed into components along two axes. We define E_s as the component of the electric field perpendicular to the plane of incidence, and E_p as the component

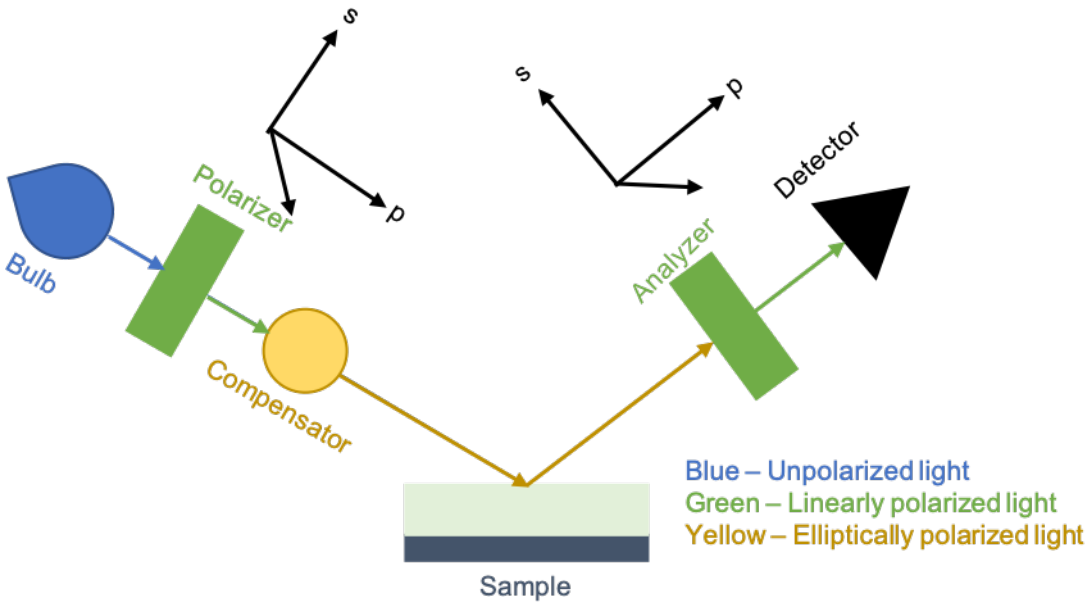

Figure 4.1: A schematic diagram of the ellipsometer. The different polarization states of the light as it travels through the system are shown.

of the field parallel to the plane of incidence, and both perpendicular to the direction of motion of the light. Each component of the elliptically polarized light has an associated phase, denoted as ξ_s and ξ_p respectively. The phase shift between the s and p components, defined as[49]

$$\delta = \xi_s - \xi_p \tag{4.1}$$

changes upon interacting with the film. We can thus define the value Δ as[49]

$$\Delta = \delta_f - \delta_i, \tag{4.2}$$

where δ_f is the final difference in phase shift of the elliptically polarized light, and δ_i is the initial difference in phase shift.

Additionally, the amplitude of the electric field, E_{0s} and E_{0p}, will be altered upon interacting with the sample film.[49] To understand how these fields are modified upon interacting with our samples, the optical model in Figure 4.2 is used. Figure 4.2 depicts our sample geometry, as

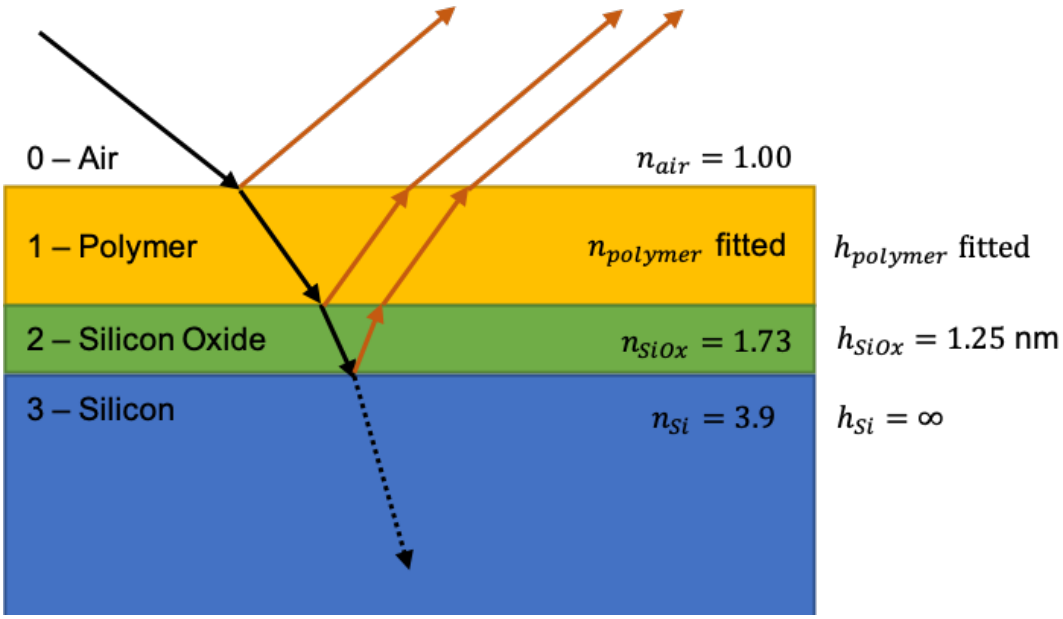

Figure 4.2: A diagram of the ellipsometry layer model used in this thesis. Literature values for the refractive index of the air, silicon oxide, and silicon are used. The height of the silicon oxide layer is 1.25 nm and the height of the silicon is treated as semi-infinite. The fit parameters are the thickness of the polymer layer and the Cauchy parameters A and B used to calculate the refractive index of the polymer.

well as how the light waves interact with the different layers. Some of the incident light at each interface is reflected, and some will be transmitted.

To simplify the explanation of how E_{0s} and E_{0p} are changed upon interacting with an interface, I will only discuss a two-layer model of our system (ignoring the silicon oxide layer). First, it is known that when light is transmitted through an interface, the transmitted light will be refracted at an angle determined by Snell's law,

$$n_0 sin(\phi_0) = n_1 sin(\phi_1), \tag{4.3}$$

where the subscripts 0 and 1 indicate any adjacent materials, such as the air and polymer layers in Figure 4.2. Additionally, ϕ indicates the angle of incidence for a given material. The light transmitted into the polymer layer will then encounter the next interface at the same angle, ϕ_1, that it was transmitted into the polymer film at. We can then define the Fresnel coefficients r_{01} such

that

$$E_0 = r_{01}E_1, \tag{4.4}$$

then the Fresnel coefficient can describe how the amplitude of a given component of the electric field changes as it propagates from medium 0, the air, to medium 1, the polymer layer.[49] We can determine the Fresnel reflection coefficients for the s or p component of light through the equations[49]

$$r_{p01} = \frac{n_1(\lambda)cos(\phi_0) - n_0(\lambda)cos(\phi_1)}{n_1(\lambda)cos(\phi_0) + n_0(\lambda)cos(\phi_1)}, r_{s01} = \frac{n_0(\lambda)cos(\phi_0) - n_1(\lambda)cos(\phi_1)}{n_0(\lambda)cos(\phi_0) + n_1(\lambda)cos(\phi_1)}, \tag{4.5}$$

which relates the Fresnel reflection coefficient for light reflecting off of the boundary between air (medium 0) and the polymer film (medium 1), r_{01}, to the angle of incidence ϕ and the wavelength-dependent refractive index $n(\lambda)$ for each medium.

The light then travels through the polymer layer and encounters the silicon layer (as we are ignoring the silicon oxide layer in this simplified example, the silicon layer will be layer 2). Once again, Equations 4.5 can be used to determine the Fresnel reflection coefficients for this interaction. An expression for the total Fresnel coefficient for the sample can be derived, and is found to be

$$r_{tot} = \frac{r_{01} + r_{12}e^{-i2\beta}}{1 + r_{01}r_{12}e^{-i2\beta}} \tag{4.6}$$

where the subscript 01 indicates the air to polymer boundary, and the subscript 12 indicates the polymer to silicon boundary.[49] This equation describes the total Fresnel reflection coefficient for either the p or s component of the polarized light. The phase thickness, β, is defined as

$$\beta = \frac{2\pi h n_1}{\lambda} cos(\phi_1). \tag{4.7}$$

where h is the thickness of the polymer layer, n_1 is the index of the polymer layer, and ϕ_1 is the angle at which the light enters the polymer film. The two quantities we are interested in finding are h and n_1.

We can define Ψ in terms of the total Fresnel reflection coefficients as[49]

$$tan(\Psi) = \frac{|r^p_{tot}|}{|r^s_{tot}|}. \tag{4.8}$$

The ellipsometer is able to measure Ψ and Δ, and we can relate these two quantities to r_{tot} and therefore to n_1 and h, using the fundamental equation of ellipsometry,[49]

$$\rho = tan(\Psi)e^{i\Delta} = \frac{r^p_{tot}}{r^s_{tot}}. \tag{4.9}$$

This equation relates the complex quantity ρ to the ratio of the Fresnel reflection coefficients of p to s polarization, where Ψ is the amplitude and Δ is the phase shift. We can then fit values for the refractive index and height of the film through minimizing the mean squared error (MSE) in our model. We model the wavelength dependence of the refractive index of the polymer n_1 using the Cauchy equation,[20,49]

$$n(\lambda) = A + \frac{B}{\lambda^2} + ..., \tag{4.10}$$

where A and B are fitting parameters, and λ is the wavelength of the light in microns.[20] We neglect the larger order terms in this expansion because of their small impact on the fit. So ultimately, our model takes in Δ and Ψ data as the temperature of the sample changes, and we use a model to extract the h, A, and B parameters, which we can use to find $n(T)$, $h(T)$, and T_g.

4.2 Ellipsometry Sample Preparation and Procedure

4.2.1 Sample Preparation

The polymers used in this thesis were produced by Rohm and Haas, a subsidiary of Dow Chemical. The fumed silica (FS) was from Cabot Corporation. Both were provided by the Parsons Conservation Lab of the Michael C. Carlos Museum of Emory University.

To make a neat sample of a polymer film for use in ellipsometry, first a 10 wt% solution of the polymer in toluene is created. A magnetic stir bar is added to the solution, and the solution is

stirred until the polymer has dissolved, usually overnight. A 2 cm by 2 cm silicon wafer piece with a 1.25 nm native oxide layer[20] is then held onto the spin-coater by vacuum, and nitrogen is blown over it to clear off any dust that may have accumulated. Toluene is then placed on the silicon, and the sample is spun until the toluene evaporates. This process further cleans the substrate. Then, a few drops of the polymer solution are placed on the silicon, and the sample is spun until the toluene in the solution evaporates off. Toluene is used as the solvent instead of acetone for spin coating, even though acetone is more commonly used in art conservation,[25,43] because acetone evaporates too fast to produce a uniform film.[23] The thickness of the dried polymer film is then measured using ellipsometry. The spin speed of the spin coater is then adjusted between 1000 - 3000 rpm to control film thickness. Next, the sample is placed in a vacuum oven at 90 °C overnight, thus annealing the polymer and evaporating off any remaining solvent. After this step, the sample is ready to be tested.

The procedure for making a sample of B-72 with some weight percent (wt%) of FS varies slightly from the procedure for neat polymers. To prepare the solution used to make the ellipsometry sample, first the required mass of FS is measured out on an analytical balance in a fume hood. Then the B-72 and toluene are added such that the B-72 is 10 wt% of the final solution. The sample is then magnetically stirred overnight. Before the sample is spun, the solution is sonicated for 5-40 minutes in order to break up FS agglomerates (as it became clear the FS agglomerates were making a rough polymer film, the sonication time was increased to further break up aggregates), and then filtered through a 0.2 micron filter to remove any remaining agglomerates. The filter should mostly remove agglomerates and not the aggregates or spheres, as the aggregates are 0.1 to 0.2 microns in length, and the spheres are 0.007 to 0.014 microns in diameter. The sample is then spun from the filtered solution. Finally, the sample is annealed under vaccuum at T_g + 20 °C = 60 °C overnight to make any remaining solvent evaporate out of the film and to relax the polymer chains.[3]

4.2.2 Measurement Procedure

Measurements for this thesis were made using a Woollam M2000 spectroscopic ellipsometer with an Instec HSC 302 hot stage. To measure the T_g, index of refraction, and thickness of the film, the sample is secured to the heating stage. Measurements are made at a 55° angle of incidence to align with previous work from our lab.[23] Measurements were taken every 10 seconds for 5 seconds. The sample is first heated to 150 °C in one minute, and held at that temperature for 20 minutes to reset its thermal history. The sample is then cooled down to 0 °C at a rate of 1 °C/min. Dry nitrogen gas at a flow rate of 1.6 L/min is run through the sample chamber to prevent condensation on the sample.

The collected Ψ and Δ data are then fit to a layer model in the CompleteEase software. The layer model is shown in Figure 4.2. The native oxide layer is held at 1.25 nm in the model and only the polymer film thickness, h, and the A and B parameters of the Cauchy equation (Equation 4.10) are allowed to vary. The data from the run is fit to the layer model, and the thickness of the polymer film, and the Cauchy parameters A and B are found at each temperature measured. The index n of the polymer is calculated using Equation 4.10 for the wavelength 589 nm, which is the yellow doublet D-line of sodium and the standard wavelength for reporting the index in art conservation.[19]

CHAPTER 5

RESULTS AND DISCUSSION OF ELLIPSOMETRY MEASUREMENTS

5.1 Ellipsometry Measurements of B-44

When I started research in the Roth lab, I contributed measurements of B-44 films by ellipsometry to a larger study by Benjamin Kasavan.[23] I present the B-44 results here to demonstrate how ellipsometry measurements of film thickness $h(T)$ and refractive index $n(T)$ as a function of temperature are used to measure the glass transition temperature T_g.

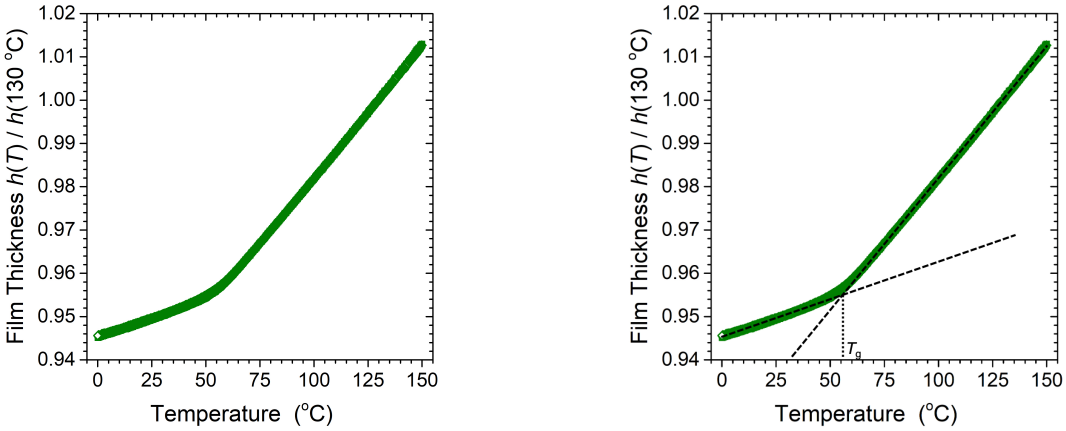

(a) (b)

Figure 5.1: (a) Normalized thickness of three samples of B-44. The thickness data from the three different samples are so similar they lie on top of each other. (b) The normalized thickness data with the lines of best fit for the high and low temperature regions superimposed as black dashed lines. The temperature at which these lines of best fit intersect is shown with a black dotted line and is labeled T_g. The T_g for this set of samples was found to be 56 ± 1 °C.[23]

B-44 films on silicon substrates were prepared and measured using the processes described in Chapter 4. All samples were between 900 and 920 nm in thickness after annealing, so all properties measured should be for bulk polymer. Figure 5.1a shows how the thickness of the film, normalized at each sample's thickness at 130 °C to enable comparisons, changed as the sample was cooled from 150 °C to 0 °C at 1 °C/minute. The linear part of the data below 45 °C was

from the polymer in its glassy state, and the linear part of the data above 70 °C comes from when the polymer was rubbery. The curved portion of the data between 45 and 70 °C comes from the polymer transitioning between the two states. The three data sets, from three different samples, lie directly on top of each other, showing great agreement between trials.

This $h(T)$ data can be used to find the glass transition temperature (T_g) of the sample through the following procedure. A line of best fit was fitted to the low-temperature $h(T)$ data, and a second line of best fit was fitted to the high-temperature $h(T)$ data. This procedure can be seen in Figure 5.1, where the dotted black lines are the linear fits. The point at which the two lines cross was determined to be the glass transition temperature T_g. The T_g of each of the samples are then averaged and the standard deviation was calculated. For this sample set, 3 samples were analyzed, and B-44 was found to have a T_g of 56 ± 1 °C.[23]

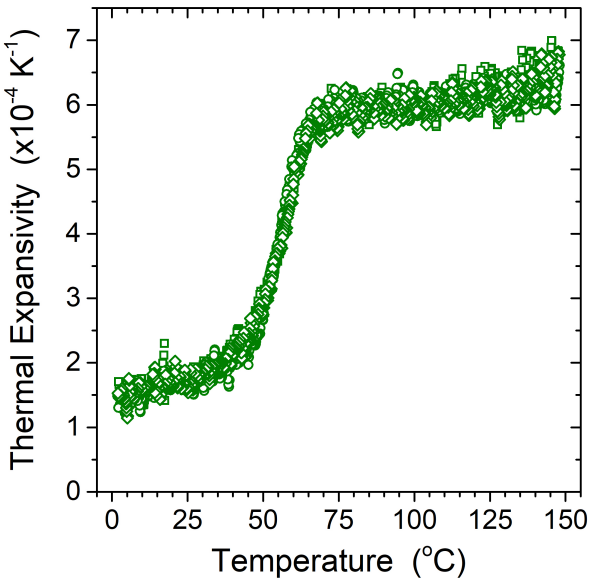

Figure 5.2: Thermal expansivity as a function of temperature for B-44. The three different data point shapes indicate three different samples, and overlap enough that they are indistinguishable.

The glass transition can be seen more clearly if we take the numerical derivative of the normalized $h(T)$ data, which is the thermal expansion (α). The thermal expansion of the polymer

was found using the numerical derivative[24]

$$\alpha = \frac{h(T + \frac{\Delta T}{2}) - h(T - \frac{\Delta T}{2})}{h(130°C) * \Delta T}, \tag{5.1}$$

where ΔT is 4.2 °C, and $h(130°C)$ is the height of the polymer film when the temperature is 130 °C. ΔT is chosen to be 4.2 °C based on previous work by Kawana and Jones, who found that this value of ΔT produced good values for α.[24] The numerical derivative of the data in Figure 5.1 is shown in Figure 5.2, which graphs the thermal expansivity of the film versus the temperature. Note that contrary to Benjamin Kasavan's thesis,[23] the thermal expansion data were not smoothed. For temperatures less than 45 °C and greater than 70 °C, the α data is approximately a flat line, as would be expected given the linear slope seen in the thickness data in Figure 5.1. In Figure 5.2 the glass transition is much more obvious, clearly occurring between 45 and 70 °C for all three samples. The slope and range of the transition data informs us about the rapidity of the transition, which can vary for different conservation adhesives.[23]

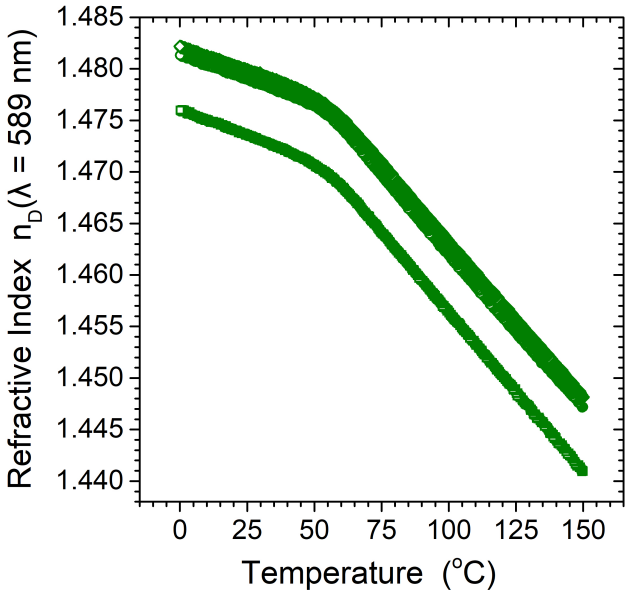

Figure 5.3: The temperature dependence of refractive index for B-44. The offset between the three different trials occurs due to differences in the initial alignment state of the ellipsometer.

The refractive index (n) is the other parameter we get from our layer model in Figure 4.2.

This data has not been normalized due to the importance of the absolute value of the refractive index to conservators when matching the adhesive to the object, however this means the refractive index is offset vertically for some samples. In his honors thesis, Benjamin Kasavan investigated this shift, and found that it was an inevitable consequence of the initial alignment state of the ellipsometer, which will often be different for different samples.[23] Thus, the best indicator of agreement of samples is seeing if the slopes of the refractive indices agree in the glassy and rubbery states, although these slopes can also vary slightly between samples of the same material. Figure 5.3 shows the refractive index of the sample for light with a wavelength of 589 nm as a function of temperature. Just like the $h(T)$ data, there are two clearly linear regimes at the high and low temperatures from this run. Around 45 to 70 °C the data curves as the polymer goes through the glass transition. Two of the data sets are very close in absolute value, whereas the square data is around 0.01 lower. However, all the data sets have the same or very similar slopes, and can thus be considered to be in good agreement.

From the refractive index data in Figure 5.3, we calculated the average and standard deviation of refractive index at room temperature (30 °C). For this data, we calculated that the index of refraction at 30 °C was 1.477 ± 0.003. This refractive index was calculated using the Cauchy equation, equation 4.10, which uses the fitting parameters A and B to produce a refractive index. Thus we can also report the average and standard deviation of A and B at room temperature. At 30 °C, A has a value of 1.463 ± 0.003 and B has a value of 0.0048 ± 0.0001 microns^2.[23]

5.2 Ellipsometry Measurements of B-72 with Different Amounts of Added Fumed Silica

We wanted to determine if the properties of B-72 change upon the addition of fumed silica (FS) to the adhesive. We investigate the temperature dependence of the refractive index and film thickness and the value of T_g using the same techniques as in Section 5.1. We made B-72 with 0 wt%, 0.2 wt%, and 0.3 wt% FS. We had to filter out agglomerates that did not break up during the sonication of the B-72 solutions with FS, so it is unknown if the 0.2 wt% and 0.3 wt% are actually that different in terms of FS content. A better way to view this data is as comparing 0 wt% (neat)

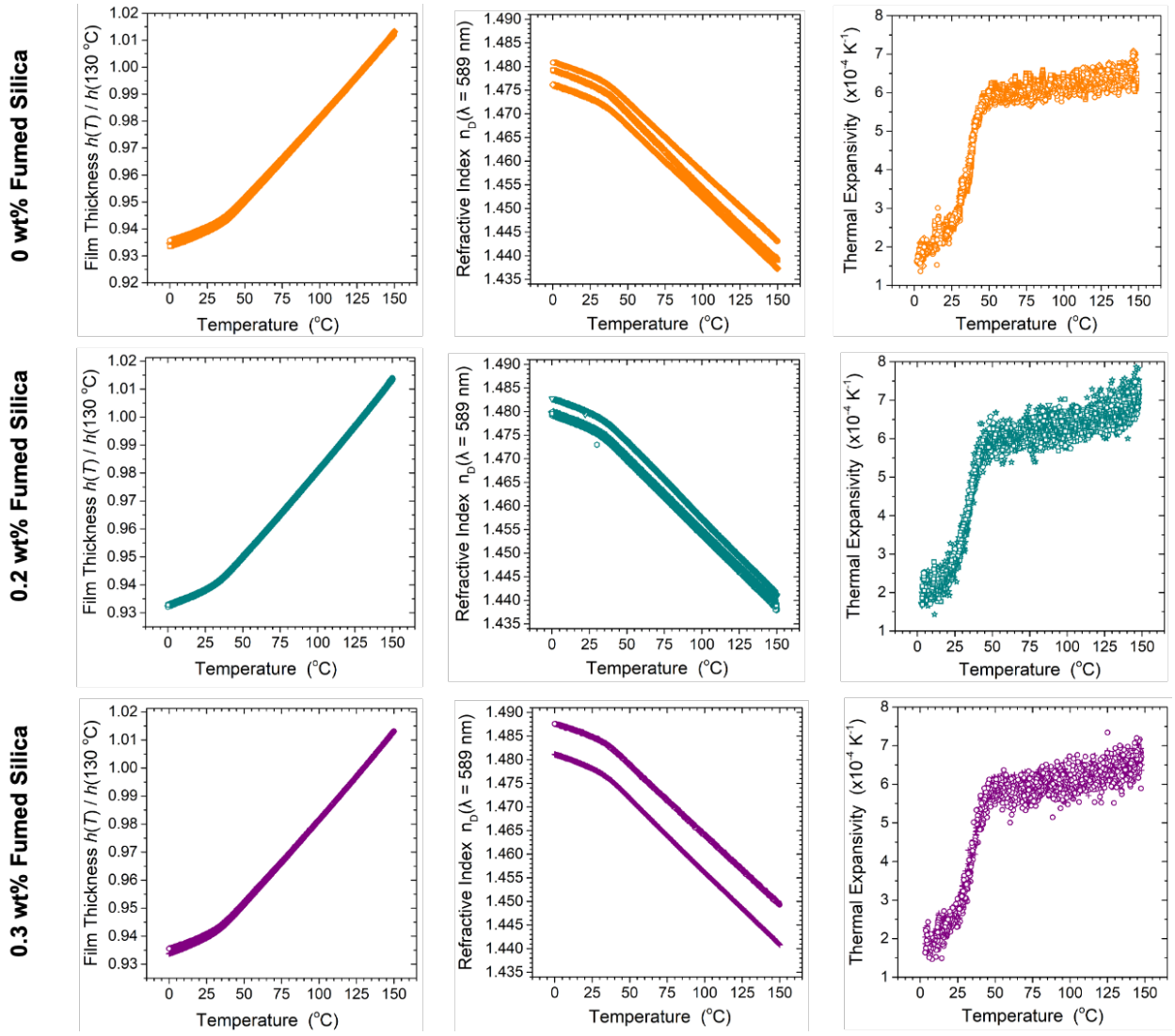

Figure 5.4: Film thickness, refractive index, and thermal expansivity data for all the B-72 ellipsometry trials. There is good agreement between the different trials for each sample set. The refractive index data has a vertical offset between some of the different trials due to differences in the initial alignment state of the ellipsometer. There are only two trails of 0.3 wt% FS due to time constraints.

B-72 to B-72 with an amount of FS on the order of 0.1 wt%.

Figure 5.4 contains the data from all the trials conducted on B-72 and B-72 with FS. The orange data is neat B-72, the teal data is B-72 with 0.2 wt% FS, and the purple data is B-72 with 0.3 wt% FS. There are only two trials of B-72 with 0.3 wt% FS due to time constraints. Each column of Figure 5.4 corresponds to a different parameter's temperature dependence. The first column is the film thickness (normalized at $h(130\ ^\circ\mathrm{C})$), the second column is the refractive

index, and the final column is the thermal expansivity. The refractive index at a given temperature varies on the order of 0.005 due to the different alignment states of the ellipsometer. However, the refractive index of historical glasses can vary on a far larger scale. For example, Roman and Egyptian glasses have been found to vary in refractive index by as much as 0.045, a whole order of magnitude larger than the variations caused by our alignment.[46] Thus, the vertical shifts along the refractive index axis in Figure 5.4 will not impact the determination of whether an adhesive's refractive index has changed enough that it effects its use in conservation. To enable comparisons between the different data sets, representative trials have been chosen from the three data sets and have been graphed together.

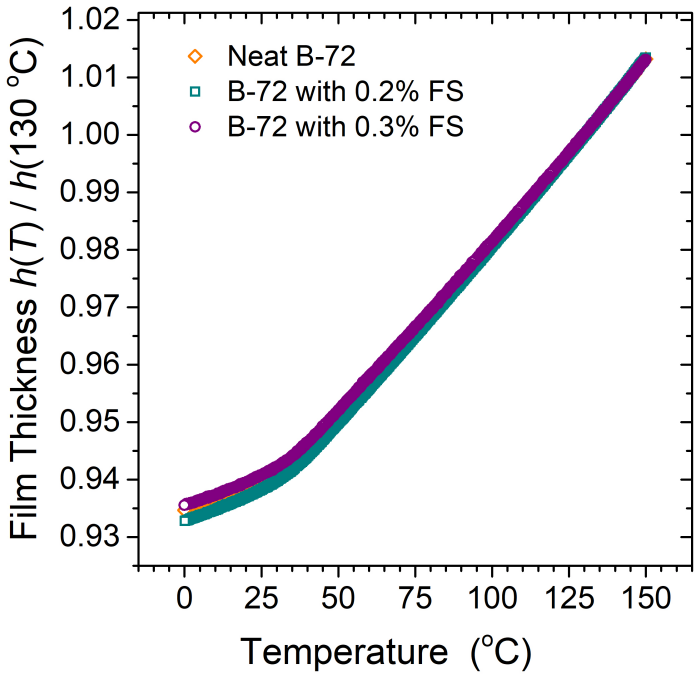

Figure 5.5: Normalized film thickness as a function of temperature for B-72 with 0 wt% (orange), 0.2 wt% (teal), or 0.3 wt% (purple) fumed silica.

Figure 5.5 depicts representative data of normalized film thickness as a function of temperature from the three different samples on the same graph. The three data sets lie on top of each other, indicating that the FS did not alter the temperature dependence of the film thickness in either the glassy or rubbery states. Additionally, the overlap indicates that the T_g of the polymer film

also could not have changed significantly with the addition of FS. This is borne out in the average values of T_g found for each concentration of FS in B-72. Neat B-72, as expected, had a T_g of 40 $\pm$ 2 °C. Samples made from B-72 with 0.2 wt% FS were found to have a T_g of 40 $\pm$ 1 °C, the same average T_g as the neat B-72 samples. Samples made from B-72 with 0.3 wt% FS had an average T_g of 38 $\pm$ 1 °C, which is lower by 2 °C than the neat and 0.2 wt% FS in B-72. We did not expect the T_g to change very much, given the literature on the subject,[42] and a 2 °C decrease is small within the context of alterations to T_g and therefore in line with our expectations. However, due to time constraints, only two samples of B-72 with 0.3 wt% FS were able to be tested. Additional data should be collected in the future so the average T_g is more likely to be representative of the true value of its T_g.

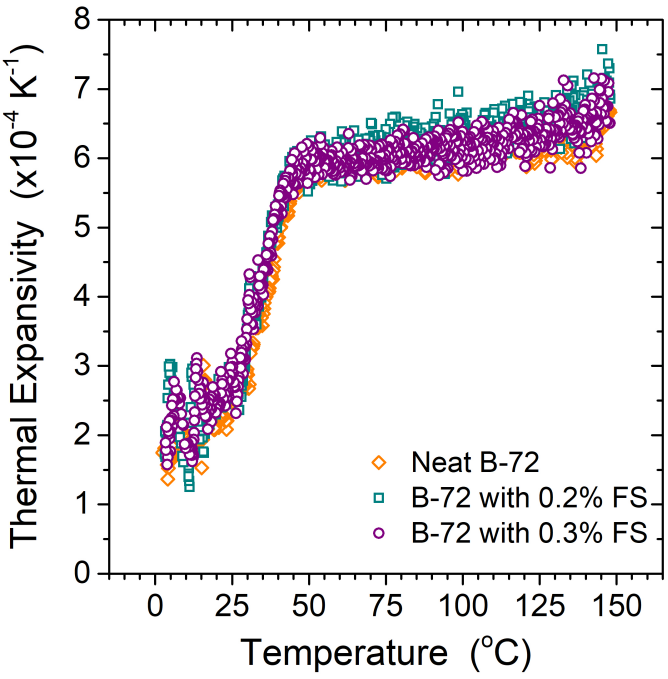

Figure 5.6: Thermal expansion as a function of temperature for B-72 with 0 wt% (orange), 0.2 wt% (teal), or 0.3 wt% (purple) FS.

Figure 5.6 compares the thermal expansions of the three loading levels of FS in B-72, which makes it much easier to see any subtle differences in their transitions. The thermal expansion of the polymer films can be found by taking the numerical derivative of the film thickness data using

Equation 5.1 as covered in the previous section. While the neat B-72 can be seen behind the B-72 with FS, there is not a sufficient difference in the behavior of the thermal expansivity during the glass transition to be able to conclude that adding the FS affected it. Additionally, the behavior of all the different samples is the same in the glassy and rubbery states. The behavior of these samples is similar enough that any difference can be considered within experimental error.

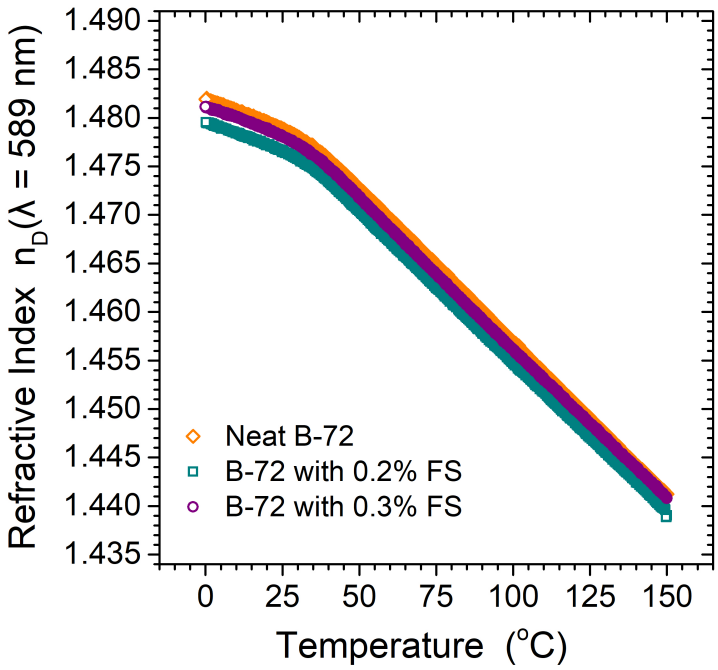

Figure 5.7: Refractive index as a function of temperature for B-72 with 0 wt% (orange), 0.2 wt% (teal), or 0.3 wt% (purple) FS.

Figure 5.7 illustrates the temperature dependence of the refractive index of B-72 with different loading levels of B-72. The slopes in the rubbery and glassy phases match between all of the samples. The similarity in refractive index of the sample data sets in Figure 5.7 is true for all the trials run on B-72. Considering the refractive index at room temperature (30 °C) for each set of samples, neat B-72 has an average refractive index of 1.475 ± 0.002, B-72 with 0.2 wt% FS has an average refractive index of 1.476 ± 0.002, and B-72 with 0.3 wt% FS has an average refractive index of 1.481 ± 0.005. Thus it seems that the addition of FS does not significantly change the refractive index of B-72.

Table 5.1 summarizes this section by comparing the number of samples, T_g, the refractive index, and the A and B values from the Cauchy equation (4.10) that were used to calculate the refractive index for each of the different loading levels of FS in B-72. Table 5.1 makes evident that there might be some small changes in T_g and n. The changes are small enough that we conclude the addition of FS did not change these properties drastically enough to impact B-72's suitability as an adhesive for conservation.

% fumed silica	**Number of samples**	T_g **in °C**	
0	3	40 ± 2	
0.2	3	40 ± 1	
0.3	2	38 ± 1	
	At room temperature, 30 °C		
% fumed silica	***n***	***A***	***B* in microns^2**
0	1.475 ± 0.002	1.462 ± 0.002	0.0046 ± 0.0002
0.2	1.476 ± 0.002	1.463 ± 0.002	0.0050 ± 0.0005
0.3	1.481 ± 0.005	1.467 ± 0.005	0.00485 ± 0.00007

Table 5.1: A comparison of the ellipsometry results for B-72 with 0 wt%, 0.2 wt%, and 0.3 wt% fumed silica.

CHAPTER 6

DESIGN OF THE CONSERVATION ADHESIVE TENSILE-TO-SHEAR (CATS) TESTER

6.1 Initial Tests to Determine Design Specifications for the Conservation Adhesive Tensile-to-Shear (CATS) Tester

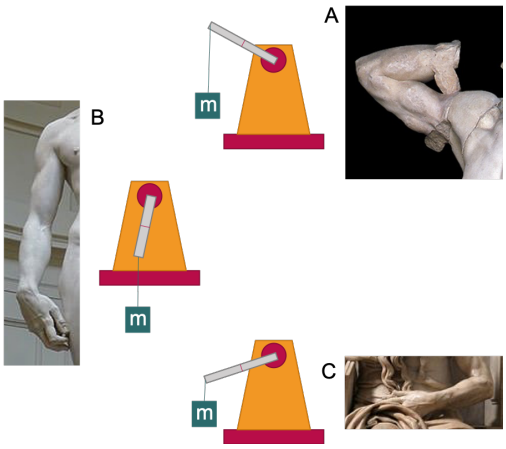

Figure 6.1: An illustration of the ability of the CATS tester to replicate the stresses that artifacts experience.[29,50,51]

For the purposes of this study we will be constructing an apparatus to measure the fracture strength of bonds. We call this apparatus the Conservation Adhesive Tensile-to-Shear (CATS) tester. We chose to build our own device to test the strength of various adhesives because we will be better able to replicate the exact mixtures of tensile and shear stress experienced by artifacts. Figure 6.1 shows how the CATS tester will be able to closely replicate the actual stresses on a bond. As mentioned in Section 3.2.4, even when the bond is perpendicular to the ground, so the force of gravity should cause a shear stress in the material, the necessary geometries of artifacts often means that the tensile strength of the bonding material still plays a large role in the fracture strength. For building the CATS tester, initial testing was done to determine the design parameters needed. The tensile fracture strength data collected from this trial is used to estimate how much weight would be needed to break the bond geometry and select the size of the bond area to use in

the CATS testing machine we constructed.

6.1.1 Sample Creation and Testing

The samples used in the initial tensile fracture stress testing were made following Koob's protocol, with a few changes based on the materials available. Toluene was used instead of the recommended acetone to enable comparisons to ellipsometry experiments. An initial solution of 2 parts toluene to 1 part B-72 was made, and 0.2 wt% of fumed silica (FS) was added. The B-72 was left to dissolve for three hours in a sealed container. At this point there were no discernible pellets of B-72 left. The solution was then sonicated for 5 minutes to further mix it and break up any agglomerates in the FS. The container was then left open in a fume hood until 50 wt% of the toluene had evaporated, giving a final solution of 1:1 toluene to B-72. The adhesive was then directly applied to the ends of the glass slides (25 mm x 1 mm x 75 mm).

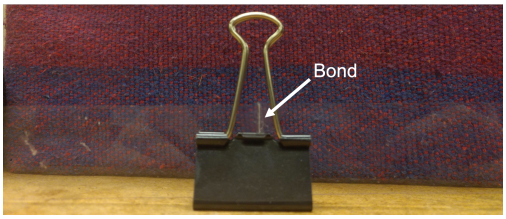

Figure 6.2: Two glass slides bonded together, being held by a paper clip as they dry. A binder clip was chosen because it was on hand and allowed air to flow around the bond.

The adhesive was applied to one end (25 mm x 1 mm) of a glass slide with a thin wooden stick. The slides were then held together end-to-end briefly, and then pulled apart to ensure all of the ends were wetted by the adhesive and to allow the solvent to evaporate more quickly. After a few seconds, the slides were put back together, and held for around a minute. Figure 6.2 shows how the slides were then clamped together with a binder clip such that the line of pressure applied by the binder clip was perpendicular to the bond. This allowed air to flow freely around the bond line to allow solvent to evaporate easily. The slides were left to dry for 48 or 96 hours, and removed from the binder clip directly before testing.

The testing apparatus for the initial tensile fracture strength tests is shown in Figure 6.3.

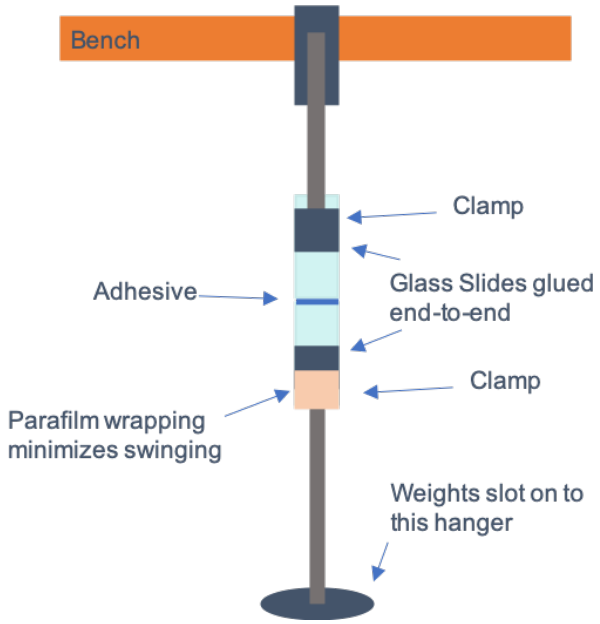

Figure 6.3: A diagram of the setup for the initial tensile fracture strength tests.

The top half of the testing device consists of a rubber-tipped clamp secured to a lab bench. The lower half of the testing device is a rubber-tipped clamp with a hanger hanging from it. The hanger was found to swing too much when weights were added, so the clamp-hanger joint was wrapped in parafilm to stabilize it. The lower half of the testing device weighed 171 g. To begin measurements, one half of the bonded sample was secured to the upper clamp. A stopwatch was started and every thirty seconds, 5 g were added to the weight hanger until the bond broke. The total weight at failure was recorded and converted to tensile fracture strength using the equation

$$\sigma_f = \frac{m_f g}{A}, \tag{6.1}$$

where σ_f is the stress at failure (fracture strength), m_f is the amount of mass that caused failure in the sample, and A is the cross-sectional area of the bond. A is 25 mm^2 for glass slides glued end-to-end like in these initial tests.

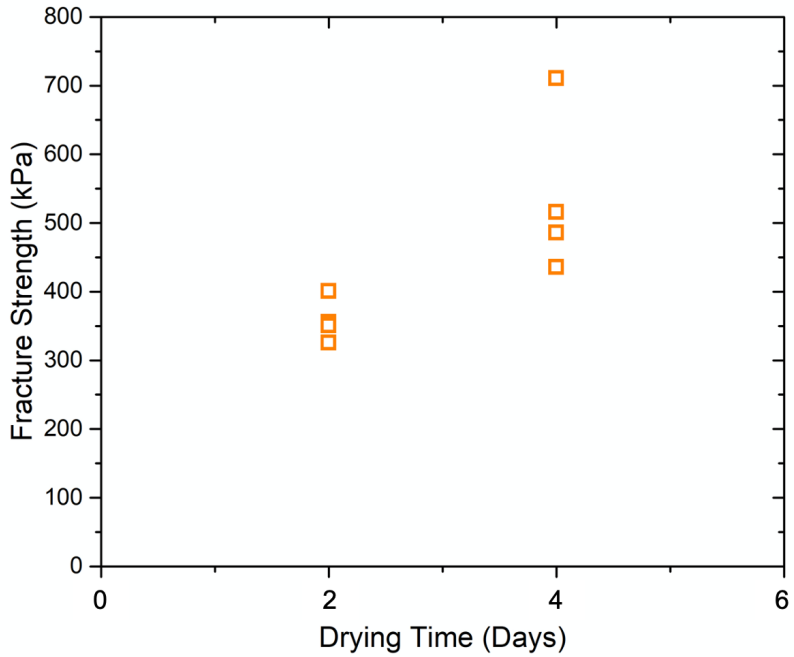

Figure 6.4: Initial results for the fracture tensile strength of B-72 (in kPa) vs drying time (in days).

6.1.2 Results from Initial Testing

In Figure 6.4 the tensile fracture strength σ_f in kPa found in Equation 6.1 is plotted against the drying time in days. Each data point is one set of glass rods that were broken by adding weights to the bottom slide. There are four data points for each drying time, although two of the samples broke at nearly the same added weight after 2 days of drying, and so one data point is nearly eclipsed by the other. The data from 4 days of drying has one data point which is higher than the rest, although not an outlier, which means the standard deviation of this set is much larger than the set of samples that were dried for 2 days. Further testing with the Conservation Adhesive Tensile-to-Shear (CATS) tester that we buit should elucidate the range of fracture strengths of B-72 with 0.2 wt% FS. While there is some overlap between the tensile fracture strengths obtained after 2 versus 4 days of drying, the increased drying time did generally increase the fracture strength of B-72 with 0.2 wt% FS.

The fracture strength data in Figure 6.4 were then plotted with data from the literature in

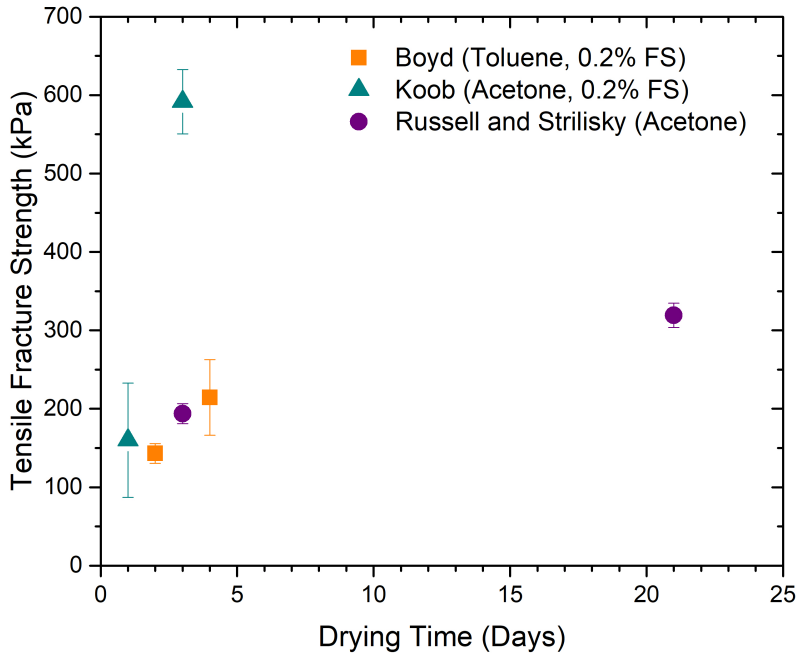

Figure 6.5: Comparison of results for the tensile fracture strength of B-72 (in kPa) vs drying time (in days). Our data, as orange squares, is compared with data from Koob[25] (teal triangles) and Russell and Strilisky[40] (purple circles). Our experiment was done with toluene and 0.2 wt% FS, Koob used acetone and 0.2 wt% FS, and Russell and Strilisky used acetone and no FS. Each data point is an average of several trials. (Koob's three day trial had a high outlier that was ignored in the calculation of the average and standard deviation of that trial.)

Figure 6.5. A summary of the experimental conditions of each different trial is delineated in Table 6.1, which shows that while Koob's and our experimental methods were very similar, Russell and Strilisky had a very different experimental setup. Each data point in Figure 6.5 is the average of all trials done by the researcher at that drying time, and the error bars show one standard deviation. The orange data is from our initial tests. The teal data is from Koob,[25] and the purple data is from Russell and Strilisky.[40] The error in our values seems smaller than that of Koob, who used the same testing procedure.[25] Russell and Strilisky had very small error bars, as they had a much larger cross sectional area they were bonding.[40] Looking at the average values of the fracture strength for each sample, our data seems comparable to the less-dried samples of Koob and Russell and Strilisky. However, Koob's data after 3 days of drying and Russell and Strilisky's data from 3 weeks of

Researcher	# of samples	Bond Size (mm)	% FS	Solvent	Substrate
Boyd	3	25 x 1	0.2	toluene	glass
Koob	3	25 x 1	0.2	acetone	glass
Russell and Strilisky (3 days)	52	50.8 x 19.05	0	acetone	limestone
Russell and Strilisky (21 days)	59	50.8 x 19.05	0	acetone	limestone

Table 6.1: A comparison of the experimental conditions of the different studies from Figure 6.5.

drying are definitely stronger than our data. This difference could arise due to the large differences in experimental design between the three data sets in Figure 6.5.

Looking first at the differences between our trial and Koob's experiment, we note that our samples were made with toluene as the solvent, which takes longer to evaporate than acetone. This was done to enable comparisons between the ellipsometry work we were doing at the time and this initial trial. However, as all of our samples failed cohesively, insufficient solvent evaporation was clearly a problem. While all of Koob's samples also failed cohesively even though he used acetone,[25] it is highly probable that more of the solvent in his samples had evaporated out, and thus his bonds were stronger. This begins to explain the very large tensile fracture stress he found at 72 hours. Koob could also have had improved results at 72 hours because he is an extremely practiced conservators who has spent his career working with glass, while this was our first foray into making a bond.

In making Figure 6.5, an outlier from Koob was not included in the average or standard deviation of his data for tensile fracture strength after three days of drying. Koob's data for three days of drying had fracture strengths of 608, 551, and 1127 kPa. The 1127 kPa sample is clearly an outlier in this context, and therefore was not included in Figure 6.5. As Koob's three-day-drying data is already much higher than the other data sets in the literature and in our initial tests, it seems likely that the 1127 kPa data point is anomalous. However, the data obtained from the CATS tester should allow us to determine if this data point is truly an outlier or if, with improved technique, it is possible to measure fracture strengths of 600 kPa and above, in which case Koob's outlier would warrant further consideration.

Secondly, there are many critical differences between our experiments and the experiments

carried out by Russell and Strilisky.[40] The Koob and Boyd data is from adhering glass slides end-to-end with a cross section of 1 mm x 25 mm,[25] whereas the Russell and Strilisky data comes from adhering limestone substrates of a much larger size (50.8 mm x 19.05 mm cross section).[40] The much larger cross section used by Russell and Strilisky will significantly slow solvent evaporation out of the bond, and likely explains the slow growth of their fracture strength over time despite using acetone, which evaporates quickly. The limestone used by Russell and Strilisky was smoothed before gluing,[40] which ensures the surface area of the bond was comparable between samples. Russell and Strilinsky claim that their limestone was not porous, so we expect their tensile fracture stress results to be reasonably comparable to our and Koob's results on glass.[40] A key difference between the Koob and Boyd data vs Russell and Strilisky's data is that Russell and Strilisky did not add any FS to their B-72.[40] Given relevant literature outlined in Chapter 3, we expect that this omission would reduce the fracture tensile stress of the bond, but we do not know if that is true for a system of B-72 and FS. Thus we cannot yet account for how the lack of FS impacted Russell and Strilisky's measurements of the fracture tensile stress of the bond.

An additional factor that must be discussed is related to the sample geometry. The long, thin bond area for the samples created by Koob and us mean that adding weights may have added some lateral force on the bond during the measurement. As weights were added, due to the setup of the testing apparatuses we used and the especially thin cross section of the bond, there would be some swinging of the bottom slide relative to the top. This added torque would serve to weaken the bond more than was taken into account in the calculation of the fracture strength. Thus, the ”true” tensile fracture strength is probably higher than measured by either Koob or us. Perhaps Koob's outlier had such a high fracture strength because there was less rocking during the experiment. The data from Russell and Strilisky comes from a larger, thicker rectangular bond geometry tested with a universal testing machine set, and thus we expect that their measured strength is as close to the ”true” fracture strength as experimentally possible.

The different bond geometries also impact the drying rate of the different experiments. The larger bonding area of Russell and Strilisky means that there is a smaller exit area (perimeter) per

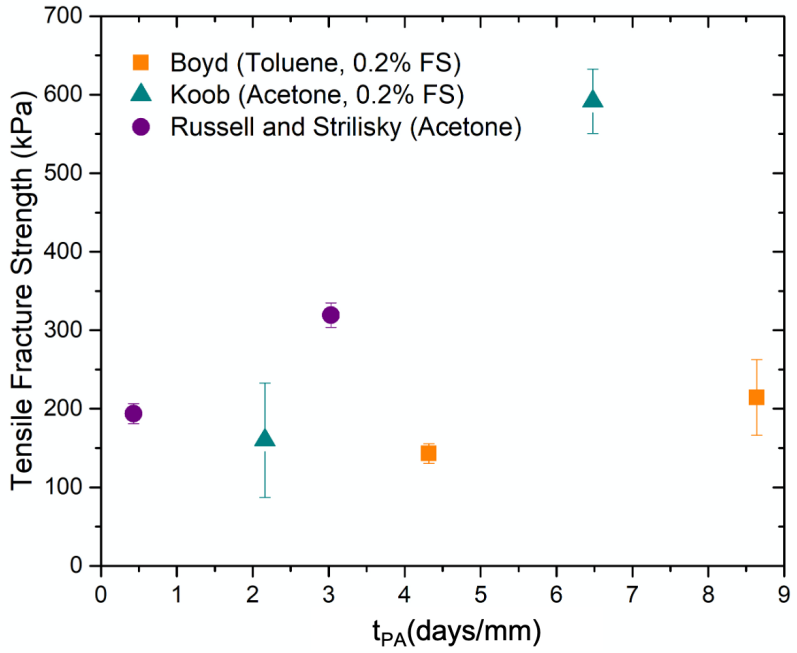

Figure 6.6: The initial results now graphed to compare the tensile fracture strength (in kPa) to the drying time per area per perimeter, called t_{PA} (see Equation 6.2) In this graph, our data in orange squares are much lower in strength than that of the Koob (in teal) and Russell and Strilisky (in purple).

bond area for the solvent to evaporate, and thus we would expect Russell and Strilisky to need to dry their samples for longer to get the same fraction of solvent evaporated out. Thus we define a new parameter, t_{PA}, which we define as

$$t_{PA} = \frac{t}{\frac{A}{P}} = \frac{tP}{A} \tag{6.2}$$

where t is the time in days the sample has dried, P is the perimeter of the bond area (in mm), and A is the bond area (in mm^2). Using this parameter we can reanalyze the data in Figure 6.5. Graphing kilopascals vs t_{PA} produces Figure 6.6.

Figure 6.6 suggests a different conclusion than Figure 6.5. Here, the effect of using toluene instead of acetone is much more obvious. Our results clearly do not match the trend of Koob's[25] and Russell and Strilisky's[40] data, as they have much higher fracture tensile strengths for a given

t_{PA}. t_{PA} will be an interesting parameter to return to when analyzing the data from the CATS tester, to see if working with acetone helps our data fit the trend established by Koob,[25] and Russell and Strilisky.[40]

Even accounting for all these differences in experimental setup between our and Koob's, and Russell and Strilisky's studies, the data in Figure 6.5 still suggests that we were able to get tensile fracture stresses in the same range as other, established conservators. However, Figure 6.6 suggests that we should have seen higher tensile fracture stress results given the geometry of our bond and how long we dried it. So while we expect the tensile fracture stress of B-72 with 0.2 wt% FS to be around 200-300 kPa for the 72 hour trials, we must design the CATS tester to be able to measure as little as 100 kPa, in case the bond is weaker in shear or with a large loading of FS. The CATS tester must also be able to measure up to and as much as 800 kPa, as adding the FS may increase the fracture strength. We will also make improvements to our application technique and will use acetone for tests with the CATS tester, which could also increase the fracture strength of the bond. The following section details how we designed the machine with these conditions in mind.

6.2 Design of the CATS Tester

We designed and constructed a machine to test the fracture strength of adhesives. For the CATS tester, stress is exerted on a bonded pair of two-inch-long segments of 6 mm borosilicate glass rods (McMaster-Carr) by adding slotted weights onto a platform hanging from the bottom half of the bonded sample at regular intervals. The top rod is attached to a Manual Rotation stage (RP01 ThorLabs), so the angle at which the bond is being tested can change. By recording the total weight added when the bond fails, the fracture strength can easily be determined.

The initial tensile fracture strength testing described in Section 6.1 helped determine the range of stress that the machine needed to be able to exert on the samples. As the amount of stress exerted on a bond given a force is dependent on the area of the bond (see Equation 6.1), we needed to ensure that the diameter of the glass rod chosen would satisfy the constraints we had. First, the

glass rods could not be thinner than 5 mm in diameter, because then they would be too fragile and more likely to break while being handled. However, the rotation stage had a max weight of 4 kg, so our rods could not be too thick or we might not be able to break them without breaking the machine. We calculated the weight that would need to be added to the machine to break the bond for 5, 6, and 7 mm diameter glass rods for a range of fracture strengths. We found that with a 6 mm diameter rod with a fracture strength of 100 kPa, around 200 g would break it. The same rod with a fracture strength of 800 kPa would require around 2200 g in added weight to break it. This amount of added weight was acceptable on both the high and low end, and so the 6 mm diameter glass rods were chosen.

The next design decision that had to be made about the CATS tester was its height. With a 6 mm diameter sample size, the hanger needed to be able to hold up to 2200 g. We calculated the resolution of the final weight added as a percentage of the total weight added for 10 to 50g. If the B-72 bond was about 100-200 kPa strong, adding 10g weights to the hanger would give us a resolution of 1.8-3.5%. From 300 to 600 kPa, the 20 g weights gave a resolution of 1.2 to 2.4%. Finally, bonds of strength greater than 600 kPa would have a resolution of 3% or less if 50 g weights were used. As all of these strengths were possible, we needed to order enough weights, in increments that would allow us to get the resolution we desired, to accommodate each of these scenarios. We ended up ordering 10 10g masses, 25 20g masses, 4 50g masses, 2 200g masses, and 2 500g masses. Additionally, once the weights were on the CATS tester they would not be taken off in order to reduce swinging of the hanger and to avoid unnecessary jostling of the sample. This made determining the height of the machine quite difficult. Heavier weights tend to have a larger radius and therefore a shorter height, but we did not want to replace the lighter, vertically costly weights mid-experiment. Thus, the hanger needed to be far longer (ultimately 15 inches) to accommodate the number of small weights that needed to be used to keep the experiment's resolution low while not replacing weights during the trial.

All of these design decisions culminated in the 3D models of the CATS tester shown in Figure 6.7. Figure 6.7a is a rendering of the base of the machine from the model design in Fusion

360. All parts of the base are made out of aluminum. The final design for the supports differs slightly from this image, as the two triangle supports have been replaced with one larger back support. Padding is placed on top of the base to lessen the sound that the weights make when the sample breaks and they fall down.

Figure 6.7b is a closeup of the 3D rendering of the portion of the machine that rotates, holds the sample, and holds the weights. The large grey square with four long screws coming out of it in Figure 6.7b is a rough model of the Manual Rotation Stage RP01 from Thor Labs. The incised circle in the block represents the part that rotates. The blue block on top of the rotating stage is made of aluminum, but colored to make the image easier to parse. The block is the upper sleeve for the sample, which can be inserted in $1\frac{1}{2}$ inches, leaving a half inch visible. The thumb screw in the middle of the block screws down to put pressure on the glass rod in the sleeve to hold it in place. The long rectangular block towards the left of Figure 6.7b is the lower sleeve of the sample, and also has a $1\frac{1}{2}$ inch slot to insert the sample into. The bottom of the lower sleeve has a hole that the hook of the hanger can fit into. The hanger is too long to be fully depicted at this angle, but it is long enough to hold a large stack of slotted weights.

Figure 6.7c shows the final 3D image of the device from Fusion 360. The base is wide enough that even when the top sleeve is rotated, the hanger still hangs over a portion of the padded base. Figure 6.8 shows an actual image of the CATS tester that was built by the machine shop.

The final thing was to cut the 24 inch glass rods we had purchased into the 2 inch segments we needed (these 2 inch segments are glued into a 4 inch sample). Alan Fannin and Horace Dale III cut the glass rods with a diamond saw, and then sanded down the end to even it out. However, the rods did not exactly match each other, so there would be some gaps in the bond, which would introduce a level of variability into our samples that we did not want. We tried scoring the rods with a diamond-tipped pen, but the curvature of the rods made that difficult. The scoring was often uneven and so produced an uneven surface area to bond. We then purchased a Scientific Glass Tubing Cutter which was made for scoring circular objects. Using this glass tubing cutter and wetting the score marks, we were able to break the rods much more cleanly than the other

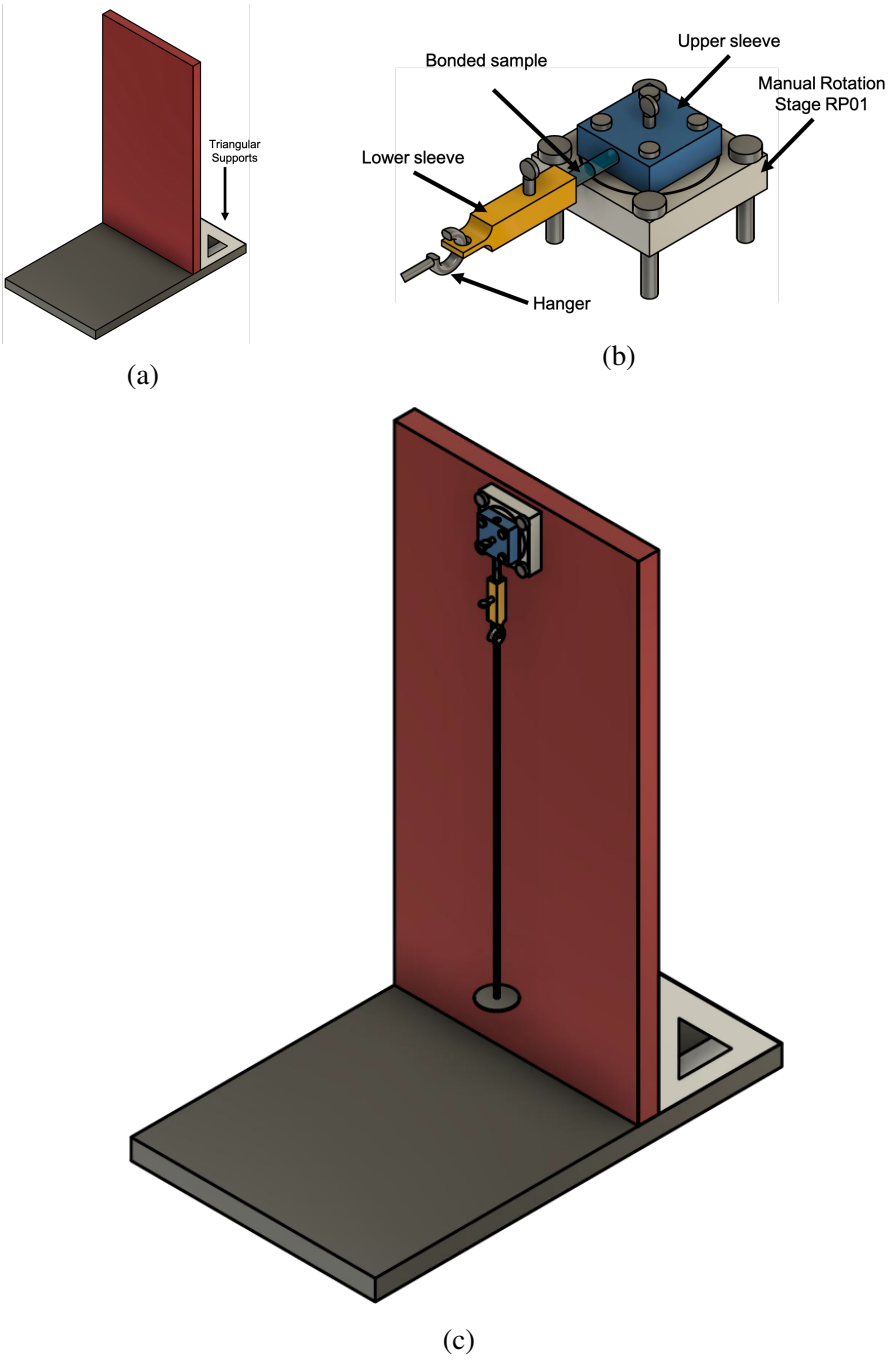

(a)

(b)

(c)

Figure 6.7: 3D models of the CATS tester. False colors were used to make the image visually easier to parse.(a) The base of the machine. The triangular supports were changed in the final design. (b) The portion of the machine that holds the sample. The manual rotation stage is in silver, the blue block holds the top of the sample, the yellow block holds the bottom of the sample and connects it to the hanger, upon which weights will be added. The screws with vertical heads are thumbscrews, which allow us to secure the glass rods in their sleeves. (c) The whole CATS tester.

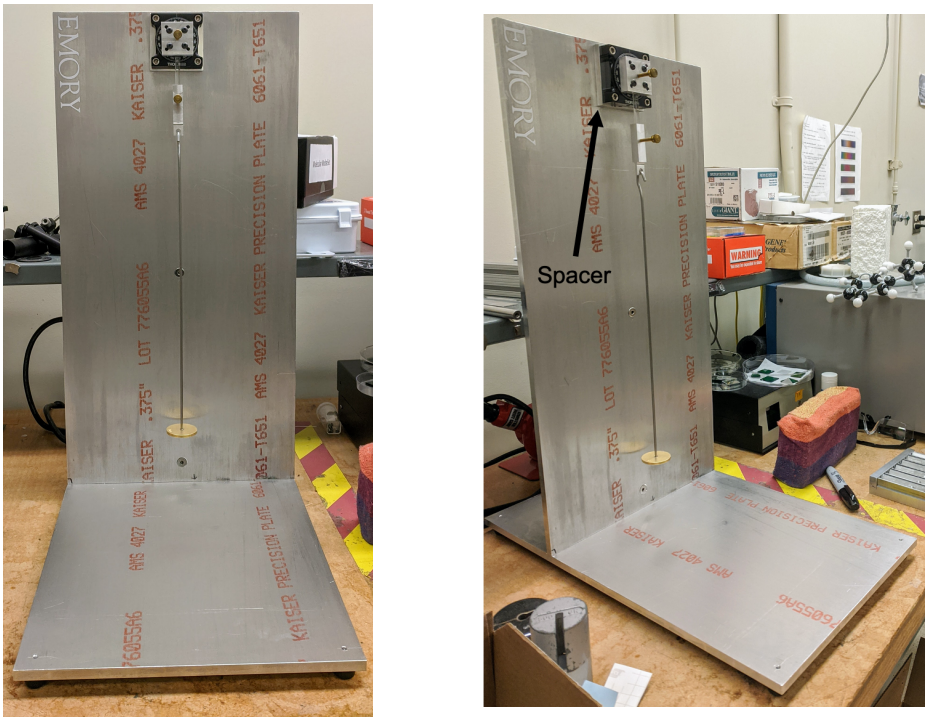

Figure 6.8: Two views of the completed testing device. The supports on the back have been changed to one larger support, and an extra spacer has been placed between the rotation stage and the back board.

methods. As there was still a ”correct” orientation for the rods relative to each other, we made a mark along the length of the rod before breaking it. By matching up the marks, a near-seamless fit could be achieved.

6.3 Design of the Drying Rack

The bonded samples need to be clamped with approximately 100 psi of pressure as they dry to produce the optimal bond.[36] The original drying rack design was based on the drying rack used in Abel's Master's thesis.[4] However, Abel's samples were much thicker than ours, and so we feared that her design might not protect our more fragile samples. Horace Dale III and Alan Fannin at the Emory Machine Shop suggested the design shown in Figure 6.9, which supports the sample through its entire length while still allowing pressure to be added and air to flow around the bond. Pressure is added to the bond through the thumb screws at the top of Figure 6.9. Since our samples are so thin, 100 psi on the bonds can be achieved with just finger strength. The bond

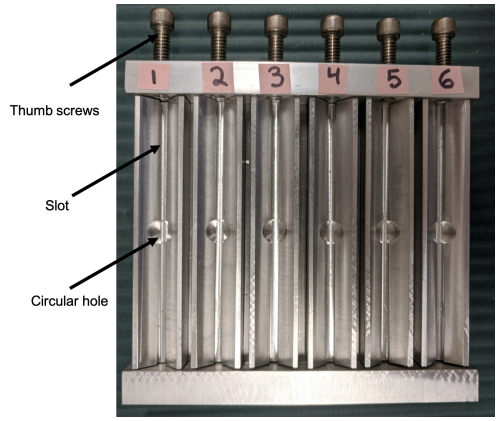

Figure 6.9: Final drying rack with labeled slots. One sample goes in each slot. A hole in the middle of each slot allows air to flow around the bond. Screws at the top of the drying rack can be tightened to put pressure on the bonds.

will rest over the circular holes in the middle of each slot, and so air will be able to flow around the whole perimeter of the bond, allowing evaporation to occur equally.

6.4 Experimental Procedure for the CATS Tester

The samples used in the initial testing with the CATS tester were made following Koob's protocol, with a few changes based on the materials available. An initial solution of 2 parts acetone to 1 part B-72 was made, and 0.2 wt% of fumed silica (FS) was added for samples that would test B-72 and FS. The B-72 was left to dissolve for one and a half hours in a sealed container. At this point there were no discernible pellets of B-72 left. The container was then left open in a fume hood until 50 wt% of the acetone had evaporated, giving a final solution of 1:1 acetone to B-72. The adhesive was then directly applied to the ends of the glass rods.

The adhesive was applied directly to one end of a glass rod with Size 0 Blick Economy Golden Taklon flat brushes. A primary coat of a more dilute solution of B-72 and acetone was not necessary for the glass rods, as they are non-porous.[45] Unlike in the initial testing, the rods were not pulled apart after they were bonded, as tack is not needed with a drying rack that supports the sample and holds the bond together as it dries. Thus we will omit this step in the sample preparation for the CATS tester.[45]

For bond application, the half of the glass rod that had no adhesive on it was already in position, laying horizontally in the drying rack. The rod with adhesive on it was placed at the other end of the sample channel, so there was space between the two rods. The rods were then pushed together through twisting the screws in the drying rack, and pressure on the join was increased until small adhesive bubbles formed along the exterior of the bond. These bubbles are easily removed after the bond dries, and clearly demonstrate that the adhesive has covered the entire bond area.[45] The samples were left to dry in the rack positioned vertically, so there would not be more adhesive dripping out of one side of the bond. Since the first question we wanted to answer with the CATS tester concerned loading levels of FS, we only wanted to test one drying time. We also wanted to make it easy to compare our results to Koob's, who dried his samples for either 1 or 3 days. We decided to dry our samples for 3 days, as we thought 1 day of drying would leave too much solvent in the bond. The samples were removed from the drying rack directly before testing.

After the 3 days, the dried adhesive bubbles on the exterior of the bonds were removed. A sample was attached to the lower sleeve of the CATS tester, and then to the upper sleeve. The lower half of the setup weighed 85 g. For the first sample in a batch, large weights are added on to the weight hanger until it breaks in order to get an estimate of the strength of the adhesive. For the remaining samples, 50% of the weight that broke the first sample is added immediately. Then, a stopwatch was started and every five seconds, 20 g was added to the weight hanger until the bond broke. If there were no more 20 g weights, 10 g weights were added every 5 seconds instead. The total weight at failure (added weight plus the hanger weight plus the lower rod's weight) was recorded and converted to tensile fracture strength using Equation 6.1. The cross-sectional area of the bond, A, is 28 mm^2 for 3 mm radius rods.

6.5 Initial Testing with the CATS Tester

Two batches of six samples, one with 0 wt% FS and one with 0.2 wt% FS, were tested with the CATS tester to determine the reproducibility of the data and see if different fracture strengths occurred for B-72 with and without 0.2 wt% FS. The amount of weight that caused each bond to

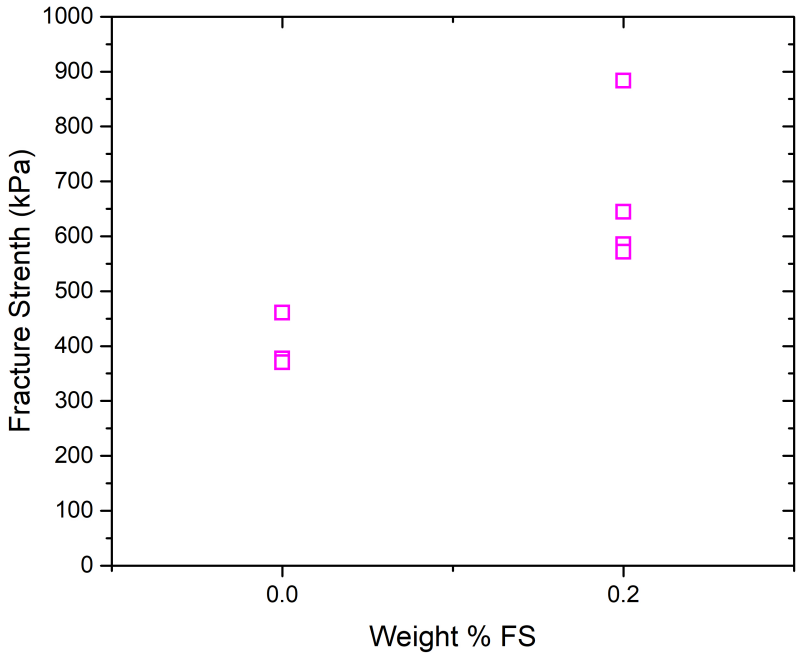

Figure 6.10: Tensile fracture strength vs weight % FS for B-72 measured with the CATS tester.

break was recorded, as well as the mass of the last weight added and the type of failure (see Figure 3.5). Equation **??** was used to calculate the fracture strength of B-72 given the amount of weight added to the tester. The tensile fracture strength versus the weight % of FS is graphed in Figure 6.10.

While six samples were made for each batch, only three to four of them resulted in meaningful data. Some samples were disqualified because they were either used to get an estimate of the strength of the bonds, and thus had low resolution, or because they broke as they were being loaded into the CATS tester. The 0.2 wt% sample that had a fracture strength of 883 kPa is shown in Figure 6.10 but will not be included in calculating the average or standard deviation of this batch, as it broke when weights were being removed from the CATS tester. Weights had to be removed as the sample as was much stronger than initially estimated, and so lower weights had to be replaced by larger weights to have enough vertical space on the hanger to increase the force on the bond. However, the strength of this sample is not an outlier. This sample qualitatively appeared to be the

best sample, as it had good alignment between the two halves of the sample and had small beads of adhesive around the bond (which were removed before testing), indicating that the right amount of adhesive was used. This suggests that the fracture strength of the B-72 with 0.2 wt% FS might be closer to the 883 kPa than the approximately 600 kPa of the other samples. As there was a fair amount of jostling of that sample as weights were added and removed, it is possible that the bond broke at a lower stress than it would have if the weights did not need to be removed. In the future, further minimizing the need to remove weights from the tester and making sure to only interact with the hanger and not the lower sleeve should prevent a bond from breaking without a known stress. Thus, 883 kPa should be considered the lower bound of the tensile fracture strength of that sample. Koob had a sample that broke at 1127 kPa, an outlier for his data. This higher fracture strength, in context with the 883 kPa fracture strength recorded with the CATS tester, indicates that the upper limit of the tensile fracture strength of B-72 with 0.2 wt% FS is not yet known. Through improving our adhesive application technique so the samples have better alignment and have been bonded with the right amount of adhesive upon securing them in the drying rack, we may be able to make stronger bonds.

While it is possible that the neat B-72 bonds could also be stronger than these initial measurements suggest due to the aforementioned reasons, I do not think their strength in future trials will increase enough that they match the strength of the bonds with FS. The batch of neat B-72 samples I made generally had very good alignment, and B-72 bubbled out of the bond slightly, indicating a good amount of adhesive was used. Additionally, there were no high outliers in the samples tested, further suggesting that the strength of neat B-72 cannot be improved too much more with better techniques.

Looking at the data in Figure 6.10, there is a clear increase in tensile fracture strength upon the addition of FS. Every single sample with 0.2 wt% has a higher fracture strength than the 0 wt% FS samples. And again, the 0.2 wt% FS samples might not be as strong as they could be as discussed previously. Thus the initial tests with the CATS tester suggests that the addition of FS to B-72 increases its tensile fracture strength. The average strength of the neat B-72 is 403 kPa,

and the average strength of the B-72 with 0.2 wt% FS is 600 kPa. The difference between the average strengths of the two batches is 197 kPa. The standard deviation for the 0 and 0.2 wt% FS batches are 39 and 41 kPa respectively, so the batch averages are 4.9 standard deviations away from each other. The standard deviation for the 0.2 wt% batch is low because the high fracture strength sample had to be excluded due to experimental error, but the average strengths are still far enough apart to argue that the addition of FS increased the tensile fracture strength of the bond, as suggested by the polymer nanocomposite literature.

To facilitate comparisons between the fracture strengths of these two batches measured with the CATS tester, the initial tests described in Section 6.1.2, and the results from the literature, the failure stresses in Figure 6.10 were averaged and used as the data point for that batch, with the standard deviation of those samples as that point's error bars. Graphing the trials from the initial testing with the CATS tester on the same graph as Figure 6.5, where the stress at failure is plotted versus the drying time for results from this thesis and the literature, we get Figure 6.11.

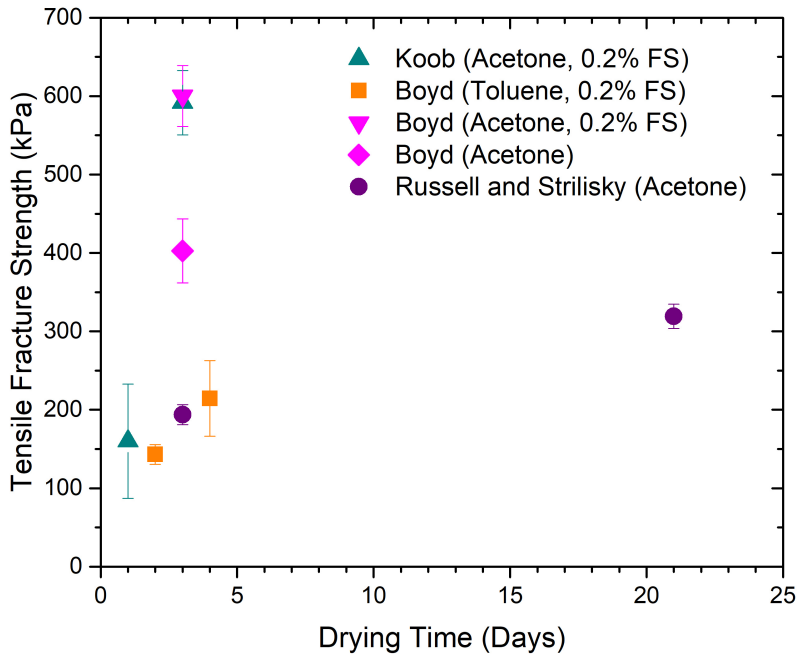

Figure 6.11: Tensile fracture strength vs drying time for B-72 measured by our initial tests, Koob's data,[25] Russell and Strilisky's data,[40] and the data from the initial tests with the CATS tester.

Figure 6.11 shows an improvement in the fracture stress between the preliminary trials conducted in this thesis and the trials using the CATS tester is clear. The preliminary tests (in orange) have average fracture stresses of 143 kPa for one day of drying and 215 kPa for three days of drying. However, the trials conducted with the CATS tester (pink) have average fracture stresses of 403 kPa for neat B-72 and 600 kPa for B-72 with FS. This increase could have been due to our improved experimental technique in adhering, drying, and testing. The increase could also be because for the tester samples we used acetone, a faster drying solvent, instead of toluene. Thus at three days, samples made with acetone would experience less of the plasticizing effects associated with trapped solvent and therefore have a higher fracture stress.

One goal of these initial trials with the CATS tester was to determine if it could produce reproducible data. The standard deviation for the two batches were 41 kPa for the B-72 with FS and 39 kPa for the neat B-72. As this standard deviation is in line with the trials done by Koob,[25] which had a standard deviation of 41 kPa, we believe this reproducibility is acceptable. Additionally, our three-day trial using Koob's procedure for making B-72 produced data that lies almost directly on top of his, so we are able to reproduce previous results from the literature.

Just like for the initial trials we did earlier in this thesis, we can graph the tensile fracture strength data vs the parameter t_{PA}, as in Figure 6.12. However, the large fracture strengths we were able to get with a t_{PA} of only around 2 means that even if we were to look only at the trials using acetone (not the orange trials), there is still no strong relationship between the t_{PA} parameter and the fracture strength of the bond, and this parameter does not seem to make these trials easier to compare. A line of best fit determined from the acetone data has an R^2 of 0.35, indicating that the t_{PA} parameter is not able to explain the relationship between the tensile fracture strength versus the drying time and the geometry of the bond.

These initial trials with the CATS tester suggest that the tester is able to produce reproducible data that matches data from the literature. These trials also suggest that the addition of FS to B-72 could change its fracture stress. However, more trials need to be done to assess the batch-to-batch variability of the samples before a firm conclusion on the relative fracture strengths

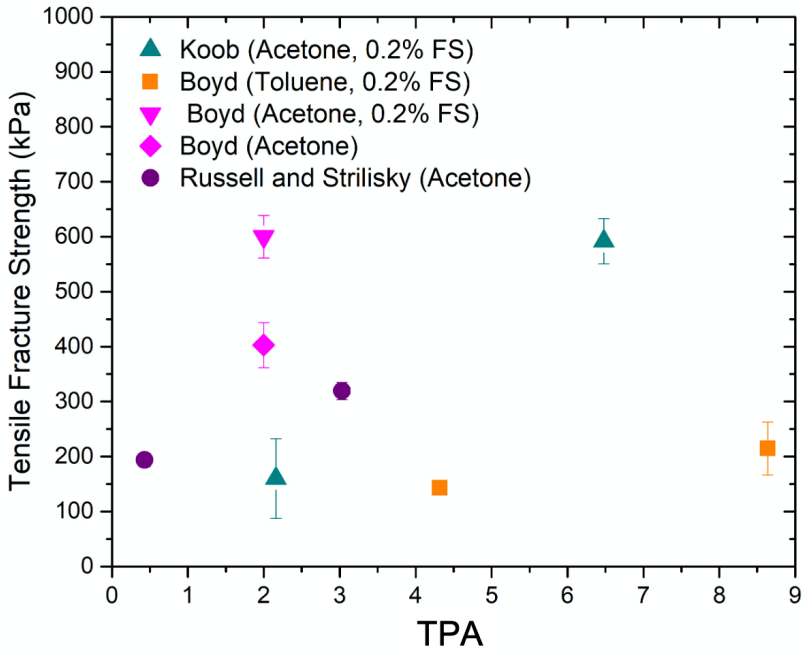

Figure 6.12: Tensile fracture strength vs t_{PA} for for B-72 measured by our initial tests, Koob's data,[25] Russell and Strilisky's data,[40] and the data from the initial tests with the CATS tester.

of B-72 with and without FS can be made.

CHAPTER 7
CONCLUSIONS AND FUTURE WORK

7.1 Conclusions

This thesis sought to determine if there were any changes to the material properties of B-72 upon the addition of fumed silica (FS). Two experimental methods were used to examine properties of B-72. First, ellipsometry was used to examine the thermal expansivity α(T), the glass transition temperature T_g, and the refractive index n(T). Then, the Conservation Adhesive Tensile-to-Shear (CATS) tester was designed and constructed to more accurately measure the fracture strength of adhesives used in art conservation. The CATS tester was specifically designed to replicate the mixture of shear and tensile stresses found in bonds in conservation.

Ellipsometry measurements of B-72 without and with 0.2-0.3 wt% FS were taken, although the exact amount of FS added was unknown as the solution had to be filtered. No meaningful change to T_g and n were observed, certainly not large enough to impact B-72's suitability for use in conservation. This conclusion needs to be supplemented by additional ellipsometry data using colloidal silica particles, which will not need to be filtered, to determine the relationship between loading % of FS to the changes in properties such as T_g.

Initial tests that sought to replicate Koob's 1986 work[25] were done to determine the specifications of the CATS tester. The CATS tester was used to test two batches of samples, one of neat B-72 and one of B-72 with 0.2 wt% FS. The standard deviation of the three samples from each batch was found to match the standard deviation of Koob's study.[25] For comparison, a high outlier (1127 kPa) was removed from Koob's (0.2 wt% FS) three day drying batch, and one of the samples from the 0.2 wt% FS with three days of drying batch that was tested with the CATS tester broke at 883 kPa upon the removal of weights. This indicates that the tensile fracture strength of B-72 with 0.2 wt% FS could be even larger than these initial tests indicate. The averages of

the two batches with and without FS were 4.9 standard deviations away from each other, with the B-72 with FS batch having a higher tensile fracture stress. This suggests that adding FS to B-72 to create a polymer nanocomposite increases the fracture stress of the material, which is in line with the literature in the polymer nanocomposite field.

7.2 Future Work

Further experiments must be done to fully understand the impact of FS on the material properties of B-72. B-72 loaded with colloidal, spherical silica will not need to be filtered in order to be examined with ellipsometry, as it was the larger than 0.2 μm agglomerates of FS that were causing the polymer films to be too rough to measure with ellipsometry, and thus making it necessary to filter the B-72 and FS solution. Thus, with colloidal silica, a clearer link between the loading level of silica and the change to the T_g, n at room temperature, or α of B-72 should be possible to determine.

Continued experiments with the CATS tester are even more important as a contribution to the conservation literature. The immediate next step for this study is to determine the batch-to-batch variability of the samples to further test the reproducibility of the experiments. Additional verification of the tensile fracture strength results with a commercial instrument will further test the reproducibility of the CATS tester's results. Then we will be able to move on to determining the effect of different preparation steps on the fracture strength of the bond. Currently, as has been explained in the graphs that compared different data sets from the literature, all tests of tensile and shear fracture strength are done with very different substrates, bonding areas, and FS loading levels. Now that the CATS tester is built and once a protocol for reproducible experiments has been established (determining if batch-to-batch variability is an issue), more impactful work can begin. By varying just one parameter, such as the amount of FS, the angle at which the stress is applied, the drying time, or the type of solvent used, we will be able to understand exactly how that one parameter influences the fracture strength of the bond. The question we will address first is the impact on tensile fracture strength of different loading levels of FS, as polymer nanocomposite

literature suggests that there is a loading level that maximizes strength, and additional FS added would actually weaken the adhesive. If we are still able to conclude that adding a small wt% of FS to B-72 increases the fracture strength of the material after more testing, FS could be avoided in adhesives for delicate pottery so the bond is not too much stronger than the artifact, and added to B-72 when monumental sculptures needed to be conserved. Therefore, a self-consistent experimental procedure and thus easily comparable body of work would inform conservators how each aspect of the adhesive preparation impacts the properties of the final bond, allowing conservators to match the material properties of the adhesive and object more accurately, and thus making the conservation process safer for the object.

REFERENCES

[1] B. J. Ash, L. S. Schadler, and R. W. Seigel, "Glass transition behavior of alumina/ polymethylmethacrylate nanocomposites," *Materials Letters*, vol. 55, no. 1-2, pp. 83–87, 2002.

[2] R. R. Baglay and C. B. Roth, "Communication: Experimentally determined profile of local glass transition temperature across a glassy-rubbery polymer interface with a T_g difference of 80 K," *Journal of Chemical Physics*, vol. 143, no. 111101, 2015.

[3] E. A. Baker, P. Rittigstein, J. M. Torkelson, and C. B. Roth, "Streamlined ellipsometry procedure for characterizing physical aging rates of thin polymer films," *Journal of Polymer Science Part B: Polymer Physics*, vol. 47, no. 24, pp. 2509–2519, 2009.

[4] J. Betz and A. G. Wheeler, "The influence of glass transition temperatures on the performance of acrylic thermoplastic adhesives," Master's thesis, Colombia University, 2017.

[5] J. L. Blackwell, M. S. Dobbins, R. E. McLay, and C. M. Truesdale, *Method of Making Fused Silica*, 5152819A, 1992.

[6] D. Boldridge, "Morphological characterization of fumed silica aggregates," *Aerosol Science and Technology*, vol. 44, no. 3, pp. 182–186, 2010.

[7] G. S. Byrne, "Adhesive formulations manipulated by the addition of fumed colloidal silica," *Studies in Conservation*, vol. 29, pp. 78–80, 1984.

[8] Cabot Corporation, personal communication, Aug. 6, 2019.

[9] P. Cassagnau, "Payne effect and shear elasticity of silica-filled polymers in concentrated solutions and in molten state," *Polymer*, vol. 44, no. 8, pp. 2455–2462, 2003.

[10] Chemical Retrieval on the Web (CROW), *Polymer properties database: Glass transition temperatures*. [Online]. Available: `http://polymerdatabase.com/polymer%20physics/Polymer%20Tg%20C.html`.

[11] S. Cheng, S. Mirigian, J. M. Y. Carrillo, V. Bocharova, B. G. Sumpter, K. S. Schweizer, and A. P. Sokolov, "Revealing spatially heterogeneous relaxation in a model nanocomposite," *Journal of Chemical Physics*, vol. 143, no. 194704, 2015.

[12] V. S. Chevali, D. R. Dean, and G. M. Janowski, "Effect of environmental weathering on flexural creep behavior of long fiber-reinforced thermoplastic composites," *Polymer Degradation and Stability*, vol. 95, no. 12, pp. 2628–2640, 2010.

[13] Edgar181, *Poly(methyl acrylate)*, Wikimedia Commons. [Online]. Available: https://commons.wikimedia.org/wiki/File:Poly(methyl_acrylate).svg.

[14] C. J. Ellison and J. M. Torkelson, "The distribution of glass-transition temperatures in nanoscopically confined glass formers," *Nature Materials*, vol. 2, no. 10, pp. 695–700, 2003.

[15] D. Erhardt, W. Hopwood, T. Padfield, and N. F. Veloz, "The Durability of Incralac: Examination of a Ten-Year Old Treatment," *Icom 7th triennial meeting. Copenhagen, 10-14 September 1984. Preprints*, 1984.

[16] R. Feller, M. Curran, and C. Baile, "Photochemical Studies of Methacrylate Coatings for the Conservation of Museum Objects," in *Photodegradation and Photostabilization of Coatings*, S. P. Pappas and F. H. Winslow, Eds., American Chemical Society, 1981.

[17] G. J. Fleer, M. A. C. Stuart, J. M. H. M. Scheutjens, T. Cosgrove, and B. Vincent, *Polymers at interfaces*, 1st ed. London: Chapman & Hall, 1998.

[18] K. M. Garland and J. C. Rogers, "The disassembly and reassembly of an egyptian limestone sculpture," *Studies in Conservation*, vol. 40, no. 1, pp. 1–9, 1995.

[19] V. Horie, *Materials for Conservation. Organic consolidant and coating*. Elsevier, 2010, ISBN: 9780750669054.

[20] X. Huang and C. B. Roth, "Changes in the temperature-dependent specific volume of supported polystyrene films with film thickness," *Journal of Chemical Physics*, vol. 144, no. 234903, 2016.

[21] N. Jouault, J. F. Moll, D. Meng, K. Windsor, S. Ramcharan, C. Kearney, and S. K. Kumar, "Bound polymer layer in nanocomposites," *ACS Macro Letters*, vol. 2, no. 5, pp. 371–374, 2013.

[22] N. Jouault, D. Zhao, and S. K. Kumar, "Role of casting solvent on nanoparticle dispersion in polymer nanocomposites," *Macromolecules*, vol. 47, no. 15, pp. 5246–5255, 2014.

[23] B. L. Kasavan, "A Study of the Physical Properties of Acrylic Polymers Commonly Used in Art Conservation," Honors Thesis, Emory University, 2019.

[24] S. Kawana and R. A. Jones, "Character of the glass transition in thin supported polymer films," *Physical Review E - Statistical Physics, Plasmas, Fluids, and Related Interdisciplinary Topics*, vol. 63, no. 021501, p. 6, 2001.

[25] S. P. Koob, "The Use of Paraloid B-72 as an Adhesive : Its Application for Archaeological Ceramics and Other Materials," *Studies in Conservation*, vol. 31, no. 1, pp. 7–14, 1986.

[26] S. P. Koob, S. Benrubi, N. A. R. van Giffen, and N. Hanna, "An old material, a new technique: casting Paraloid B-72 for filling losses in glass," *Symposium 2011: Adhesives and Consolidants for Conservation: research and applications: proceedings = Adhésifs et consolidants pour la conservation: recherche et applications: les actes*, pp. 1–14, 2011.

[27] C. Krumrine and L. Kronthal, "What a relief! A practical, inexpensive approach to the conservation of a large 19th Dynasty sandstone stela," *Objects Specialty Group Postprints*, vol. 3, pp. 21–38, 1995.

[28] S. K. Kumar, V. Ganesan, and R. A. Riggleman, "Perspective: Outstanding theoretical questions in polymer-nanoparticle hybrids," *Journal of Chemical Physics*, vol. 147, no. 020901, 2017.

[29] LivioAndronico, *Laocoon and his sons*, Licensed under Creative Commons Attribution-Share Alike 3.0 Unported (http://creativecommons.org/licenses/bysa/3.0/), Wikimedia Commons. [Online]. Available: `https://commons.wikimedia.org/wiki/File:Laocoon_and_His_Sons.jpg`.

[30] H. Lu and S. Nutt, "Restricted relaxation in polymer nanocomposites near the glass transition," *Macromolecules*, vol. 36, no. 11, pp. 4010–4016, 2003.

[31] D. Maillard, S. K. Kumar, B. Fragneaud, J. W. Kysar, A. Rungta, B. C. Benicewicz, H. Deng, L. C. Brinson, and J. F. Douglas, "Mechanical properties of thin glassy polymer films filled with spherical polymer-grafted nanoparticles," *Nano Letters*, vol. 12, no. 8, pp. 3909–3914, 2012.

[32] A Moncrieff, "Protecting silver from tarnishing," *IIC News*, vol. 4, no. 2, pp. 6–7, 1966.

[33] E. E. Nagy, "Fills for White Marble: Properties of Seven Fillers and Two Thermosetting Resins," *Journal of the American Institute for Conservation*, vol. 37, no. 1, p. 69, 1998.

[34] J. F. Podany, K. M. Garland, W. R. Freeman, and J. Rogers, "Paraloid B-72 as a Structural Adhesive and as a Barrier within Structural Adhesive Bonds : Evaluations of Strength and Reversibility," *Journal of the American Institute for Conservation*, vol. 40, no. 1, pp. 15–33, 2001.

[35] *Poly(ethyl methacrylate), also known as PEMA*, Wikimedia Commons. [Online]. Available: `https://commons.wikimedia.org/wiki/File:Poly(ethyl_methacrylate),_also_known_as_PEMA.jpg`.

[36] C. Riccardelli, M. Morris, G. Wheeler, J. Soultanian, L. Becker, and R. Street, "The treatment of Tullio Lombardo's Adam: A new approach to the conservation of monumental marble sculpture," *Metropolitan Museum Journal*, vol. 49, no. 1, pp. 48–116, 2014.

[37] P. Rittigstein and J. M. Torkelson, "Polymer–Nanoparticle Interfacial Interactions in Polymer Nanocomposites: Confinement Effects on Glass Transition Temperature and Suppression of Physical Aging," *Journal of Polymer Science*, vol. 44, no. 20, pp. 2935–2943, 2006.

[38] C. B. Roth, Ed., *Polymer Glasses*. CRC Press, 2017, ISBN: 9781498711876.

[39] C. B. Roth and J. R. Dutcher, "Glass transition temperature of freely- standing films of atactic poly(methyl methacrylate)," *The European Physical Journal E*, vol. 12, pp. 103–107, 2003.

[40] R. Russell and B. Strilisky, "Keep it together: An evaluation of the tensile strengths of three select adhesives used in fossil preparation," *Collection Forum*, vol. 30, no. 1-2, pp. 85–95, 2016.

[41] Sigma-Aldrich Co., *Fumed Silica Product Information*. [Online]. Available: https://www.sigmaaldrich.com/content/dam/sigma-aldrich/docs/Sigma/Product_Information_Sheet/1/s5130pis.pdf.

[42] F. W. Starr, J. F. Douglas, D. Meng, and S. K. Kumar, "Bound Layers "Cloak" Nanoparticles in Strongly Interacting Polymer Nanocomposites," *ACS Nano*, vol. 10, no. 12, pp. 10 960–10 965, 2016.

[43] R. A. Stein, personal communication, Jul. 2019.

[44] ——, personal communication, Jan. 22, 2020.

[45] ——, personal communication, Feb. 28, 2020.

[46] N. H. Tennent and J. H. Townsend, "The significance of the refractive index of adhesives for glass repair," *Studies in Conservation*, vol. 29, no. sup1, pp. 205–212, 1984.

[47] The Dow Chemical Company, "Technical data sheet for Acetone from Dow," p. 2, 2012. [Online]. Available: http://msdssearch.dow.com/PublishedLiteratureDOWCOM/dh_08ac/0901b803808aca04.pdf?filepath=oxysolvents/pdfs/noreg/327-00041.pdf&fromPage=GetDoc.

[48] M. F. Thees, J. S. McGuire, and C. B. Roth, "Review and Reproducibility of Forming Adsorbed Layers From Solvent Washing of Melt Annealed Films," *submitted to Soft Matter*, January 8, 2020.

[49] H. G. Tompkins, *A User's Guide to Ellipsometry*. Academic Press: San Diego, CA, 1993.

[50] J. B. Unna, *David by michelangelo*, Licensed under Creative Commons Attribution 3.0 Unported (https://creativecommons.org/licenses/by/3.0/deed.en), Wikimedia Commons. [On-

line]. Available: https://commons.wikimedia.org/wiki/File:%27David%27_by_Michelangelo_Fir_JBU002.jpg.

[51] ——, *'moses' by michelangelo*, Licensed under Creative Commons Attribution 3.0 Unported (https://creativecommons.org/licenses/by/3.0/deed.en), Wikimedia Commons. [Online]. Available: https://commons.wikimedia.org/wiki/File:%27Moses%27_by_Michelangelo_JBU140.jpg.

[52] US National Library of Medicine, *Compound summary: 2-vinylpyridine*. [Online]. Available: https://pubchem.ncbi.nlm.nih.gov/compound/2-vinylpyridine.

[53] A. Vinçotte, E. Beauvoit, N. Boyard, and E. Guilminot, "Effect of solvent on PARALOID® B72 and B44 acrylic resins used as adhesives in conservation," *Heritage Science*, vol. 7, no. 1, pp. 1–9, 2019.

[54] M. Webb, "Methods and Materials for Filling Losses on Lacquer Objects," *Journal of the American Institute for Conservation*, vol. 37, no. 1, p. 117, 1998.

[55] K. I. Winey and R. A. Vaia, "Polymer Nanocomposites," *MRS Bulletin*, vol. 32, no. April, pp. 314–322, 2007.

[56] J. Wolfe, "Effects of bulking paraloid B-72 for marble fills," *Journal of the American Institute for Conservation*, vol. 48, no. 2, pp. 121–140, 2009.

[57] Wouterhagens, *Vergelijk nanodeeltje*, Licensed under Creative Commons Attribution-Share Alike 3.0 Unported (http://creativecommons.org/licenses/bysa/3.0/), Wikimedia Commons. [Online]. Available: https://commons.wikimedia.org/wiki/File:Vergelijk_nanodeeltje.jpg.

[58] D. Zhao, S. Ge, E. Senses, P. Akcora, J. Jestin, and S. K. Kumar, "Role of Filler Shape and Connectivity on the Viscoelastic Behavior in Polymer Nanocomposites," *Macromolecules*, vol. 48, no. 15, pp. 5433–5438, 2015.